

ornl



3 4456 0147977 8

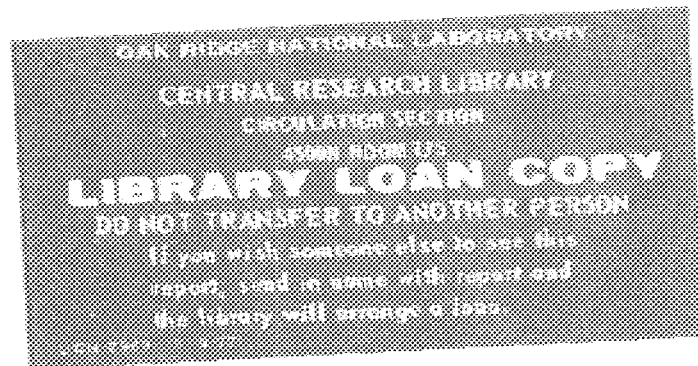
ORNL/TM-10150

**OAK RIDGE
NATIONAL
LABORATORY**

MARTIN MARIETTA

Theory of Resistive Pressure-Gradient-Driven Turbulence

B. A. Carreras
L. Garcia
P. H. Diamond



OPERATED BY
MARTIN MARIETTA ENERGY SYSTEMS, INC.
FOR THE UNITED STATES
DEPARTMENT OF ENERGY

Printed in the United States of America. Available from
National Technical Information Service
U.S. Department of Commerce
5285 Port Royal Road, Springfield, Virginia 22161
NTIS price codes—Printed Copy: A04; Microfiche A01

This report was prepared as an account of work sponsored by an agency of the United States Government. Neither the United States Government nor any agency thereof, nor any of their employees, makes any warranty, express or implied, or assumes any legal liability or responsibility for the accuracy, completeness, or usefulness of any information, apparatus, product, or process disclosed, or represents that its use would not infringe privately owned rights. Reference herein to any specific commercial product, process, or service by trade name, trademark, manufacturer, or otherwise, does not necessarily constitute or imply its endorsement, recommendation, or favoring by the United States Government or any agency thereof. The views and opinions of authors expressed herein do not necessarily state or reflect those of the United States Government or any agency thereof.

ORNL/TM-10150
Dist. Category UC-20g

Fusion Energy Division

**THEORY OF RESISTIVE
PRESSURE-GRADIENT-DRIVEN TURBULENCE**

B. A. Carreras

L. Garcia

P. H. Diamond

Institute for Fusion Studies, The University of Texas, Austin

Date Published: November 1986

Prepared by the
OAK RIDGE NATIONAL LABORATORY
Oak Ridge, Tennessee 37831
operated by
MARTIN MARIETTA ENERGY SYSTEMS, INC.
for the
U.S. DEPARTMENT OF ENERGY
under Contract No. DE-AC05-84OR21400



3 4456 0147977 8

CONTENTS

ABSTRACT	v
I. INTRODUCTION	1
II. RESISTIVE INTERCHANGE MODE STABILITY MODEL	5
III. LINEAR STABILITY PROPERTIES	9
IV. RENORMALIZED THEORY OF RESISTIVE PRESSURE-GRADIENT-DRIVEN TURBULENCE	17
V. SOLUTION OF THE RENORMALIZED EQUATIONS FOR THE RESISTIVE PRESSURE-GRADIENT-DRIVEN TURBULENCE	25
VI. THREE-DIMENSIONAL NUMERICAL CALCULATIONS OF RESISTIVE PRESSURE-GRADIENT-DRIVEN TURBULENCE	31
VII. CONCLUSIONS	41
ACKNOWLEDGMENT	43
REFERENCES	45

ABSTRACT

Saturated resistive pressure-gradient-driven turbulence is studied analytically and with numerical calculations. Fluid viscosity and thermal diffusivity are retained in the analysis and calculations. Such dissipation guarantees the existence of a stable, high- m dissipation range, which serves as an energy sink. An accurate saturation criterion is proposed. The resulting predicted pressure diffusivity scales similarly to the mixing length estimate but is significantly larger in magnitude. The predictions of the analytic theory are in good quantitative agreement with the numerical results for fluctuation levels.

I. INTRODUCTION

Resistive pressure-gradient-driven turbulence, which evolves from linear resistive interchange instabilities,^{1,2} is a likely cause of fluctuations and anomalous transport in magnetically confined plasmas. Indeed, resistive interchange modes have been proposed as the cause of anomalous thermal transport in stellarators³ and reversed-field pinches,^{4,5} while the closely related resistive ballooning mode has been proposed as an explanation of the degraded energy confinement in high- β_p tokamak plasmas with auxiliary heating.⁶ Thus, the development of an understanding of resistive pressure-gradient-driven turbulence is a generic theoretical problem of broad interest.

Previous work on the theory of resistive pressure-gradient-driven turbulence has consisted primarily of the application of mixing length arguments⁴ and dimensional analysis techniques.⁵ Mixing length arguments, such as $D = \gamma/k_x^2$, attempt to relate the properties of fully evolved turbulence to the characteristic scales of the underlying linear instability by semiquantitatively balancing nonlinearity with the linear drive. Dimensional analysis techniques utilize the scale transformation symmetries of the basic, nonlinear equations. Both yield similar results for predicted fluctuation levels, diffusivities, etc. These predictions are in qualitative agreement with the results of numerical simulations performed for relatively high resistivity and high viscosity. The agreement was particularly good for predicted scalings with β_p , dp_0/dr , etc. However, when compared directly with experimental results, the predicted thermal diffusivities were, in general, too small to explain the observed phenomena.

There are several deficiencies in the theoretical underpinnings of the mixing length and dimensional analysis approaches. First, as mentioned earlier, mixing length predictions are derived from a heuristic procedure of balancing nonlinearity with linear drive. In particular, no genuine saturation criterion based on considerations of energetics is satisfied or even established. Second, the dimensional analysis

approach, as implemented in Ref. 5, omits the effects of dissipation and the role of scales dominated by dissipative damping. The omission of damping, which is analogous to lack of a well-defined saturation criterion, explains why the (zero damping) mixing length predictions agree with those of dimensional analysis.

An initial attempt to resolve these difficulties was undertaken in Ref. 7. In that work, a saturation criterion was defined in terms of the requirement that fluctuation energies be stationary in time, and the thermal dissipation required for this was retained in the analysis. A two-point spectrum theory, which treated the nonlinear coupling of sources and sinks, was developed. Quantitative calculations indicated an enhancement of the predicted turbulence levels beyond those given by mixing length theory. The leading order parameter scalings of the predicted diffusivity agreed with those of mixing length theory. The nonlinear radial correlation length was determined by the asymptotic balance of turbulent viscosity with resistive field line bending. The saturation levels were determined by the balance of the nonlinearly modified curvature drive (i.e., diffusion was retained in the \hat{p} response calculation) with resistive field line bending. It was also shown that the enhancement factor is determined by the effective Reynolds number of the resistive pressure-gradient-driven turbulence.

Despite the progress it reflected, Ref. 7 still contained two significant deficiencies. First, large- m resolution and pressure gradient control were insufficient in the numerical calculations. Thus, only qualitative tests of the nonlinear theory were possible. Second, the analytical theory did not include collisional viscosity effects in the vorticity evolution equation. As shown here, collisional viscosity is required to stabilize short-wavelength, fast interchange modes and thus provide an energy sink. Note that gradient-flattening effects in the simulation obscured the significance of this omission.

In this paper, saturated resistive pressure-gradient-driven turbulence is studied analytically and with numerical calculations. Fluid viscosity and thermal diffusivity

are retained in the analysis and calculations. The viscosity and thermal diffusivity guarantee the existence of a stable large- m dissipation range, which serves as an energy sink. In the numerical calculation, the pressure gradient is held fixed, thus avoiding possible confusion of quasilinear and nonlinear effects. Sufficient large- m resolution is retained, and the existence of a saturated state is demonstrated by well-converged numerical calculations. A saturation criterion is proposed. This criterion requires the turbulence level to be high enough that energy outflow, as represented by renormalized fluid viscosity and pressure diffusivity, from the energy-containing low- m modes is sufficient to stabilize these modes. *The resulting predicted pressure diffusivity scales similarly to the mixing length estimate but is significantly larger in magnitude.* The parameter scalings of the enhancement factor are determined. The predictions of the analytic theory are in good quantitative agreement with the results of the numerical calculations. The implications of the results for fluctuation levels and particle transport in stellarators are discussed.

A similar departure from the simple mixing length theory was found for the resistivity-gradient-driven turbulence.⁸ In that case, at saturation, the level of diffusion adjusts to a value at which thermal dissipation balances resistivity gradient drive. Finally, it is worthwhile to note that in a recent study⁹ of ion temperature-gradient-driven turbulence due to η_i modes, related considerations also lead to a significant enhancement of saturated turbulence levels beyond the levels corresponding to mixing length predictions.

The remainder of the paper is organized in the following manner. The basic resistive pressure-gradient-driven turbulence model is presented in Sec. II. In Sec. III, the linear stability properties of the model are investigated, with particular emphasis on the role of the dissipative terms. In Sec. IV, the renormalized theory of the resistive pressure-gradient-driven turbulence is developed. A simplified set of renormalized equations is derived. They are analytically solved in Sec. V. The saturation mechanism and the significance of the mixing length approach are discussed.

Section VI contains a discussion of the multiple-helicity nonlinear numerical results and comparisons with the analytic theory predictions. Finally, Sec. VII contains the summary and conclusions.

II. RESISTIVE INTERCHANGE MODE STABILITY MODEL

The basic resistive g -mode stability is discussed in this section. The equations used for the multiple-helicity numerical calculations are presented. For the analytic calculations, a simplified electrostatic model is used. The approximations made in deriving such a model are also discussed in this section, with special attention given to the implications of conservation laws.

The simple model of the resistive interchange instability used in this paper contains the main physics properties of the instability, while taking the average pressure gradient as the only source of free energy. The basic geometry is a periodic cylinder of length $L = 2\pi R_0$. The model consists of three equations:

$$\frac{\partial \psi}{\partial t} = -R_0 \nabla_{\parallel} \phi + R_0 \eta J_Z \quad , \quad (1)$$

$$\frac{dU}{dt} = -\frac{1}{\rho_m} \nabla_{\parallel} J_Z + \frac{1}{\rho_m} \mathbf{z} \cdot (\nabla \Omega \times \nabla \tilde{p}) + \mu \nabla_{\perp}^2 U \quad , \quad (2)$$

$$\frac{d\tilde{p}}{dt} = \chi_{\perp} \nabla_{\perp}^2 \tilde{p} - V_r \frac{dp_0}{dr} \quad . \quad (3)$$

Here ψ is the poloidal flux, ϕ the velocity stream function, and $p = p_0 + \tilde{p}$ the total pressure, where p_0 is the time-averaged pressure and \tilde{p} the fluctuating part. The term $V_r(dp_0/dr)$ in Eq. (3) is shown explicitly because it contains the only free-energy source term, dp_0/dr . To simulate the conditions of steady-state turbulence, dp_0/dr is maintained constant in time throughout the calculations presented here.

The vorticity is $U = \nabla_{\perp}^2 \phi$, and $J_Z = \nabla_{\perp}^2 \psi / (\mu_0 R_0)$ is the current parallel to the z -axis of the cylinder. For the initial equilibrium the current density is taken to be zero. The constant μ_0 is the vacuum permeability. The convective derivative is

$$\frac{d}{dt} = \frac{\partial}{\partial t} + \mathbf{V} \cdot \nabla \quad , \quad (4)$$

with the velocity given in terms of the stream function by $\mathbf{V} = \nabla \phi \times \mathbf{z}$, and the derivative along the magnetic field lines is ∇_{\parallel} , where

$$\nabla_{\parallel} f = \frac{1}{R_0} (\mathbf{z} \times \nabla \psi) \cdot \nabla f + B_0 \frac{\partial f}{\partial z} \quad , \quad (5)$$

and B_0 is the magnetic field along the z -direction, which we assume to be constant. The coefficients η , μ , and χ_\perp are the collisional resistivity, viscosity, and cross-field thermal transport coefficients, respectively. They multiply the corresponding dissipative terms in Eqs. (1)–(3). Finally, ρ_m is the constant mass density.

This model, as stated, can be interpreted as the reduced magnetohydrodynamic (MHD) equations¹⁰ for a straight stellarator configuration. This reduced set of equations can be derived using the stellarator expansion.¹¹ From this viewpoint, the $\nabla\Omega$ term can be interpreted as the average helical curvature, and it is directly related to the oscillating part of the external stellarator field \mathbf{B}_v by

$$\Omega = \frac{1}{B_0^2} \overline{|\mathbf{B}_v|^2} . \quad (6)$$

Here the bar indicates toroidal angle average. In the present calculations, Ω is taken to be a function of r only and is constant in time.

Equations (1)–(3) constitute the basic model used in the present studies. They are solved numerically by the nonlinear initial value KITE code.¹² The results are discussed in detail in Sec. VI. For the analytic calculations, we have used a simplified electrostatic model that results from neglecting the induced electric field ($\partial\psi/\partial t$) term in Eq. (1). Then Ohm's law is simplified to

$$J_Z = \frac{1}{\eta} \nabla_{\parallel}^{(0)} \phi , \quad (7)$$

and the model reduces to two equations,

$$\frac{dU}{dt} = -\frac{1}{\eta\rho_m} \nabla_{\parallel}^{(0)2} \phi + \frac{1}{\rho_m} \mathbf{z} \cdot [\nabla\Omega \times \nabla\tilde{p}] + \mu \nabla_{\perp}^2 U , \quad (8)$$

$$\frac{d\tilde{p}}{dt} = \chi_{\perp} \nabla_{\perp}^2 \tilde{p} - \frac{1}{r} \frac{\partial\phi}{\partial\theta} \frac{dp_0}{dr} . \quad (9)$$

Here $\nabla_{\parallel}^{(0)}$ means that only the equilibrium magnetic field is included in the parallel derivative. From Eqs. (1)–(3) one can derive equations for the evolution of the magnetic energy,

$$E_M = \frac{1}{2R_0^2\mu_0} \int dV |\nabla_{\perp}\psi|^2 , \quad (10)$$

the kinetic energy,

$$E_K = \frac{\rho_m}{2} \int dV |\nabla_{\perp} \phi|^2, \quad (11)$$

and the mean-square pressure fluctuation,

$$E_p = \frac{1}{2} \int dV \tilde{p}^2. \quad (12)$$

These evolution equations are

$$\frac{dE_M}{dt} = \int dV J_Z \nabla_{\parallel} \phi - \eta \int dV J_Z^2, \quad (13)$$

$$\frac{dE_K}{dt} = - \int dV J_Z \nabla_{\parallel} \phi + \int dV V_r \tilde{p} \frac{d\Omega}{dr} - \mu \rho_m \int dV U^2, \quad (14)$$

$$\frac{dE_p}{dt} = -\chi_{\perp} \int dV |\nabla_{\perp} \tilde{p}|^2 - \int dV V_r \tilde{p} \frac{dp_0}{dr}, \quad (15)$$

for rigid conductive boundary conditions. The terms with $\nabla_{\parallel} \phi$ in Eqs. (13) and (14) transform kinetic energy into magnetic energy, the latter being dissipated by resistive diffusion. The kinetic energy is driven by the radial flux of pressure across curved magnetic field lines. Part of the kinetic energy is expended by coupling to magnetic energy, and part is dissipated by viscosity. The averaged pressure fluctuation is driven by the radial flux of pressure and damped by cross-field dissipation.

By a slight change in the definition of E_p ,

$$\bar{E}_p = \frac{1}{2} \int dV \frac{\tilde{p}^2}{|(dp_0/dr)(d\Omega/dr)^{-1}|} \quad (16)$$

has the dimensions of energy, and its evolution equation,

$$\frac{d\bar{E}_p}{dt} = -\chi_{\perp} \int dV \frac{|\nabla_{\perp} \tilde{p}|^2}{|(dp_0/dr)(d\Omega/dr)^{-1}|} - \int dV V_r \tilde{p} \frac{dp_0/dr}{|(dp_0/dr)(d\Omega/dr)^{-1}|}, \quad (17)$$

can be combined with Eqs. (13) and (14) to yield a global energy conservation equation,

$$\begin{aligned} \frac{d}{dt} (E_M + E_K + \bar{E}_p) &= \int dV V_r \tilde{p} \frac{d\Omega}{dr} \left[1 - \frac{(dp_0/dr)(d\Omega/dr)^{-1}}{|(dp_0/dr)(d\Omega/dr)^{-1}|} \right] \\ &\quad - \eta \int dV J_Z^2 - \mu \rho_m \int dV U^2 \\ &\quad - \chi_{\perp} \int dV \frac{|\nabla_{\perp} \tilde{p}|^2}{|(dp_0/dr)(d\Omega/dv)^{-1}|}. \end{aligned} \quad (18)$$

If $(dp_0/dr)(d\Omega/dr)^{-1} < 0$, the first term in Eq. (18) drives the energy while the other three dissipate total energy. If $(dp_0/dr)(d\Omega/dr)^{-1} > 0$, there are no driving terms. It is clear from this discussion that the only source of free energy for the instability is the pressure gradient in the bad curvature region. If this term is kept constant in time, a steady state is only possible by balancing the driving term with dissipative terms. As the latter are only effective for small scale lengths, energy transfer through a turbulent spectrum is required to attain such a steady state. Conversely, without dissipative terms, no steady-state situation can be attained.

III. LINEAR STABILITY PROPERTIES

The linear stability properties of resistive interchange modes are discussed in this section. Special emphasis is given to the effect of dissipative terms because of the impact they have on nonlinear stability properties and their role in determining the attainability of steady-state turbulence.

The resistive interchange modes are radially localized.^{1,2} Therefore, a sheared-slab approximation gives a good description of their linear stability properties. In the linear approximation, the eigenfunctions can be expressed as

$$\begin{aligned}\phi &= \tilde{\phi}_m(r) \sin\left(m\theta + n\frac{z}{R_0}\right), \\ \tilde{p} &= \tilde{p}_m(r) \cos\left(m\theta + n\frac{z}{R_0}\right).\end{aligned}$$

Setting $x = r - r_s$, where r_s is the radial position of the singular surface, $q(r_s) = m/n$, the linearized form of Eqs. (8) and (9) is

$$\frac{\partial}{\partial t} \left(\nabla_{\perp}^2 \tilde{\phi}_m \right) = \mu \nabla_{\perp}^4 \tilde{\phi}_m - \frac{1}{\rho_m} \frac{d\Omega}{dr} \frac{m}{r_s} \tilde{p}_m + \frac{m^2}{\eta} \frac{B_0^2}{\rho_m R_0^2} \frac{x^2}{q^2 L_q^2} \tilde{\phi}_m, \quad (19)$$

$$\frac{\partial \tilde{p}_m}{\partial t} = -\frac{m}{r_s} \frac{dp_0}{dr} \tilde{\phi}_m + \chi_{\perp} \nabla_{\perp}^2 \tilde{p}_m. \quad (20)$$

Here $L_q = |(1/q)(dq/dr)|^{-1}$ and all radial derivatives are taken at $r = r_s$. The operator ∇_{\perp}^2 in the present approximation is given by

$$\nabla_{\perp}^2 \equiv \frac{d^2}{dx^2} - \frac{m^2}{r_s^2}. \quad (21)$$

It is convenient to write Eqs. (19) and (20) in dimensionless form by changing the variables in the following way: $X = mx/r_s$, $P_m = \tilde{p}_m m (dp_0/dr)^{-1} r_s^{-1}$, and $\Phi_m = \tilde{\phi}_m \tau_R / a^2$. Here, a is the radius of the cylinder and $\tau_R = a^2 \mu_0 / \eta$ is the resistive skin time. Then Eqs. (19) and (20) become

$$\bar{\mu} \frac{d^4 \Phi_m}{dX^4} - (\bar{\gamma} + 2\bar{\mu}) \frac{d^2 \Phi_m}{dX^2} + (\bar{\gamma} + \bar{\mu} + K_2 X^2) \Phi_m + K_1 P_m = 0, \quad (22)$$

$$\bar{\chi}_{\perp} \frac{d^2 P_m}{dX^2} - (\bar{\gamma} + \bar{\chi}_{\perp}) P_m - \Phi_m = 0, \quad (23)$$

with $\bar{\chi}_\perp = \tau_R \chi_\perp / a^2$, $\bar{\mu} = \tau_R \mu / a^2$, and $\bar{\gamma} = r_s^2 \gamma \tau_R / (a^2 m^2)$. The coefficients K_1 and K_2 are

$$K_1 = \left(a \frac{d\Omega}{dr} \right) \left(\frac{r}{am} \right)^4 \frac{\beta_0}{2\epsilon^2} \left(\frac{-a}{p_0(0)} \frac{dp_0}{dr} \right) S^2 , \quad (24)$$

$$K_2 = m^2 \left(\frac{r}{am} \right)^6 \left(\frac{a}{qL_q} \right)^2 S^2 \left(\frac{a^2 \mu_0}{\tau_R \eta} \right) , \quad (25)$$

where $S \equiv \tau_R / \tau_{hp}$ is the ratio of the resistive time to the poloidal Alfvén time, $\tau_{hp} = R_0 \sqrt{\mu_0 \rho_m} / B_0$. The parameter $\epsilon = a / R_0$ is the inverse aspect ratio of the cylinder, and $\beta_0 = 2\mu_0 p_0(0) / B_0^2$ is the peak beta value. Equations (22) and (23), together with the boundary condition on P_m and Φ_m , define a sixth-order eigenvalue problem with $\bar{\gamma}$ the eigenvalue. The problem can be simplified using cosine Fourier transforms. In this way, the system of Eqs. (22) and (23) is reduced to the following second-order eigenvalue problem:

$$\frac{d^2 \hat{\phi}_m}{dy^2} = \frac{1}{K_2} \left[\bar{\mu} (1 + y^2)^2 + \bar{\gamma} (1 + y^2) - \frac{K_1}{\bar{\gamma} + \bar{\chi}_\perp (1 + y^2)} \right] \hat{\phi}_m , \quad (26)$$

where

$$\hat{\phi}_m(y) = \int_0^\infty dX \Phi_m(X) \cos(Xy) . \quad (27)$$

The eigenvalue problem (26) can be solved by the WKB approximation. It is, in general, a two-turning-point problem. Therefore, the eigenvalue condition can be written as

$$\frac{2}{(K_2)^{\frac{1}{2}}} \int_0^{y_0} dy \sqrt{\frac{K_1}{\bar{\gamma} + \bar{\chi}_\perp (1 + y^2)} - \bar{\gamma} (1 + y^2) - \bar{\mu} (1 + y^2)^2} = \frac{\pi}{2} , \quad (28)$$

with y_0 being the positive real root of the integrand, that is, the solution of

$$\bar{\mu} \bar{\chi}_\perp (1 + y_0^2)^3 + \bar{\gamma} (\bar{\mu} + \bar{\chi}_\perp) (1 + y_0^2)^2 + \bar{\gamma}^2 (1 + y_0^2) = K_1 . \quad (29)$$

This equation can be viewed as a cubic equation for $\bar{y}_0 \equiv (1 + y_0^2)$. The condition equivalent to the instability condition is $K_1 > 0$; for large enough K_1 , the cubic equation has a positive real root. Therefore, under these conditions, when $\bar{y}_0 > 1$

there is a single real positive value of y_0 satisfying Eq. (29), and Eq. (26) is a two-turning-point problem. Let us first consider the case with only resistive dissipation, that is, $\bar{\mu} = \bar{\chi}_\perp = 0$. In this case, the integral in Eq. (28) can be calculated, and Eq. (28) yields the dispersion relation

$$\bar{\gamma}_m^{(0)2} + \bar{\gamma}_m^{(0)\frac{3}{2}} K_2^{\frac{1}{2}} = K_1 . \quad (30)$$

The superscript (0) in the growth rate refers to the $\bar{\mu} = \bar{\chi}_\perp = 0$ case. For high S values and low m modes, $K_1 \gg 1$ and $K_2 \gg 1$. Therefore, the second term on the left-hand side of Eq. (30) dominates the first, and $\bar{\gamma}_m^{(0)} \approx (K_1^2/K_2)^{\frac{1}{3}}$. In this limit, we recover the well-known $\eta^{\frac{1}{3}}$ growth rate for the resistive interchange mode. In terms of physical parameters, the growth rate is

$$\gamma_m^{(0)} = \left(\frac{\tau_R \eta}{a^2 \mu_0} \right)^{\frac{1}{3}} \left[\frac{\beta_0}{2\epsilon^2} \left(a \frac{d\Omega}{dr} \right) \left(\frac{-a}{p_0(0)} \frac{dp}{dr} \right) \frac{mqL_q S}{r_s^2} \right]^{\frac{2}{3}} \tau_R^{-1} . \quad (31)$$

For very high m modes, the first term on the left-hand side of Eq. (26) dominates the second one. In this limit, $\bar{\gamma}_m^{(0)} \approx K_1^{\frac{1}{2}}$, this growth rate corresponds to the so-called fast interchange mode. In terms of the physical parameters, $\gamma_m^{(0)}$ is given by

$$\gamma_m^{(0)} = \left[\frac{\beta_0}{2\epsilon^2} \left(a \frac{d\Omega}{dr} \right) \left(\frac{-a}{p_0(0)} \frac{dp_0}{dr} \right) \right]^{\frac{1}{2}} \tau_{hp}^{-1} . \quad (32)$$

The growth rate of the mode no longer depends on resistivity in this limit. We have plotted the growth rates given by the dispersion relation, Eq. (28), and by the two limiting expressions, Eqs. (31) and (32), in Fig. 1a. The growth rates have been calculated using the equilibrium parameters in Table I, with $\beta_0/2\epsilon^2 = 0.0125$ and $S = 10^5$. The dispersion relation (28) gives a good description of the resistive interchange instability in the limit of $\bar{\mu} = \bar{\chi}_\perp = 0$. For the more general case, the dispersion relation has been tested by comparing the growth rate given by Eq. (28) with the numerically calculated value obtained from the linearized equations (1)–(3) solved by KITE.¹² In Fig. 1b, the results of this comparison are plotted. The calculations are done for the same parameters as in Fig. 1a.

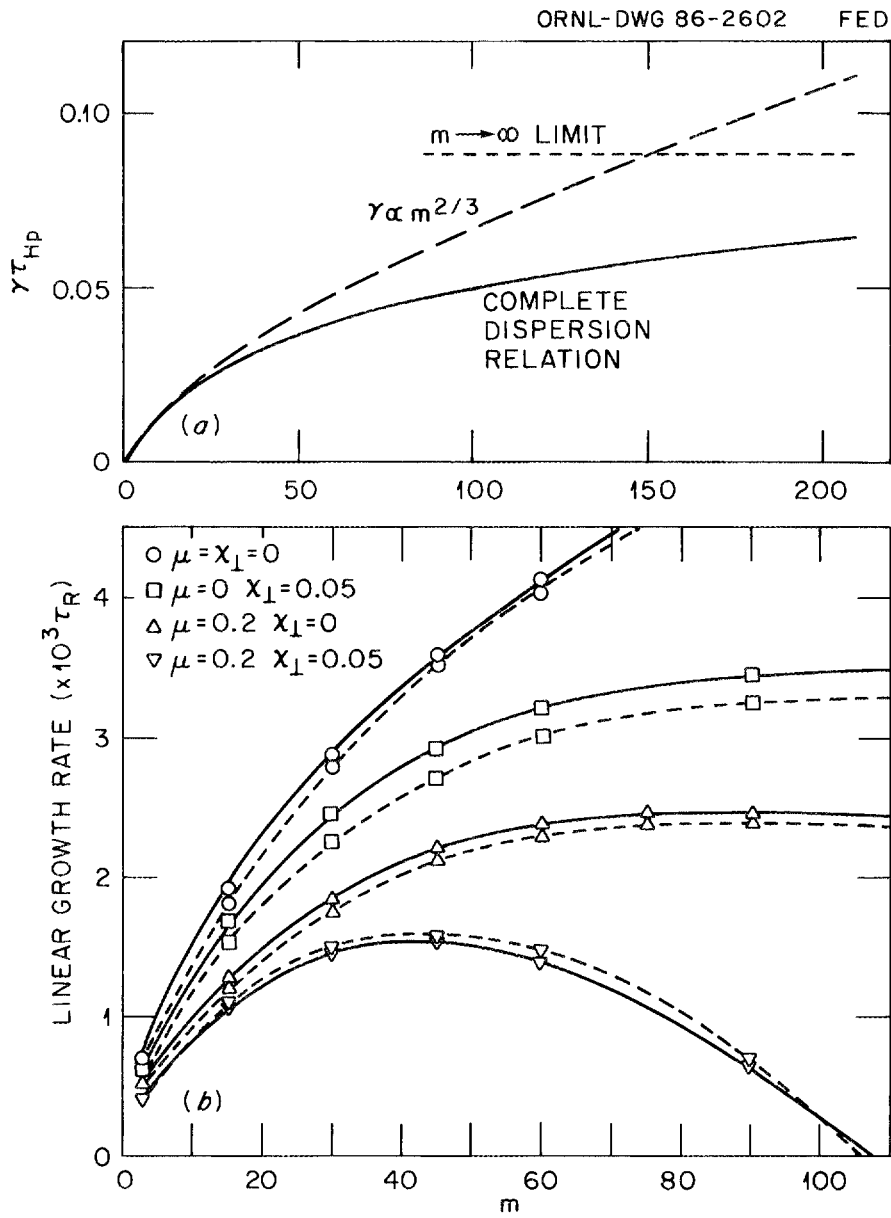


FIG. 1. Linear growth rates of resistive interchange modes as a function of the mode number.

Table I. Physical parameters at $q(r_s) = 3/2$ relevant to the resistive interchange stability calculations presented in this paper

Parameters	Values
r_s	0.5228
q	1.5
L_q	1.275a
$a \frac{d\Omega}{dr}$	0.436
$p_0(r_s)$	0.6246
$\frac{a}{p_0(0)} \frac{dp_0}{dr}$	-1.4127

Figure 1b shows that the high- m mode can be stable if both $\bar{\mu}$ and $\bar{\chi}_\perp$ are different from zero. This is a general result, which is important because it has implications bearing on the nonlinear evolution of the resistive interchange turbulence. To reach a saturated steady state, it is necessary to have an effective energy sink at high m . This energy sink exists only if the high- m modes, above a critical m value m_c , are linearly stable. The value of m_c is finite only if both $\bar{\mu}$ and $\bar{\chi}_\perp$ are different from zero. For a given mode number m , the values of μ and χ_\perp to stabilize this mode can be calculated from Eq. (28) by setting $\bar{\gamma} = 0$ in that equation:

$$\frac{\pi}{4} \left(\frac{K_2}{\bar{\mu}} \right)^{\frac{1}{2}} = \int_0^{y_0} dy \sqrt{\frac{K_1}{\bar{\mu}\bar{\chi}_\perp} \frac{1}{1+y^2} - (1+y^2)^2} . \quad (33)$$

Given either $\bar{\mu}$ or $\bar{\chi}_\perp$, this equation can be regarded as the eigenvalue condition for the other. In this limit, $y_0 = \left[(K_1/\bar{\mu}\bar{\chi}_\perp)^{\frac{1}{3}} - 1 \right]^{\frac{1}{2}}$. It is clear from the expressions for y_0 that unless $\bar{\mu}$ and $\bar{\chi}_\perp$ are both nonzero, there is no solution to Eq. (33). The integral in Eq. (33) cannot, in general, be calculated in a simple way. However, for a relevant range of parameters, high S and low m , $(K_1/\bar{\mu}\bar{\chi}_\perp)^{\frac{1}{3}} \gg 1$, the integral in Eq. (33) can be calculated in an approximate way and yields

$$\bar{\chi}_{\perp c} = \frac{K_1}{K_2} \left\{ \frac{4}{\pi} \ln \left[2 \left(\frac{K_1}{\bar{\chi}_{\perp c} \bar{\mu}_c} \right)^{\frac{1}{6}} \right] \right\}^2. \quad (34)$$

The subscript c indicates that the $\bar{\chi}_{\perp}$ and $\bar{\mu}$ values are the critical values for marginal stability. The ratio K_1/K_2 can be calculated from Eqs. (24) and (25),

$$\begin{aligned} \frac{K_1}{K_2} &= \frac{\beta_0}{2\epsilon^2} \left(a \frac{d\Omega}{dr} \right) \left(\frac{-a}{p_0(0)} \frac{dp_0}{dr} \right) \left(\frac{qL_q}{r} \right)^2 \frac{\tau_R \eta}{a^2 \mu_0} \\ &= \gamma_m^{(0)} W_m^{(0)2}. \end{aligned} \quad (35)$$

Here, $\gamma_m^{(0)}$ and $W_m^{(0)}$ are the linear growth rate and width of the linear eigenfunction in absence of dissipation ($\bar{\mu} = \bar{\chi}_{\perp} = 0$ case); $\gamma_m^{(0)}$ is the solution of Eq. (28), and $W_m^{(0)}$ can be calculated by balancing the inertia term with the field line bending term in Eq. (19), yielding:

$$W_m^{(0)} = \left[\frac{\beta_0}{2\epsilon^2} \left(a \frac{d\Omega}{dr} \right) \left(\frac{-a}{p_0(0)} \frac{dp_0}{dr} \right) \right]^{\frac{1}{6}} \left(\frac{\tau_R \eta}{a^2 \mu_0} \frac{1}{S} \right)^{\frac{1}{3}} \left(\frac{q^2 L_q^2}{mar} \right)^{\frac{1}{3}} a. \quad (36)$$

The term $\gamma_0 W_0^2$ could be considered the logical estimate for $\bar{\chi}_{\perp c}$ based on dimensional analysis. The extra dimensionless factor in Eq. (34) strongly enhances the value of $\gamma_0^{(0)} W_m^{(0)2}$ at low m and low values of dissipation. The enhancement factor is approximately an order of magnitude. In spite of its logarithmic functional dependence, it gives a strong m dependence to $\bar{\chi}_{\perp c}$ (Fig. 2).

The stabilization of the high- m modes, $m \geq m_c$, results not from radial dissipation effects but from the poloidal dissipation. For the case with $\bar{\mu} \neq 0$ and $\bar{\chi}_{\perp} \neq 0$, the radial scale length W is larger than $W_m^{(0)}$, due to the broadening of the eigenfunction caused by radial diffusion. At high m , $W > r/m$, which corresponds to the fast interchange regime. Therefore, retaining only the poloidal scale length in Eqs. (19) and (20), it is possible to derive the value of m for marginal stability, m_c :

$$m_c \simeq \left[\frac{S^2}{\bar{\mu} \bar{\chi}_{\perp}} \left(\frac{r}{a} \right)^4 \frac{\beta_0}{2\epsilon^2} \left(a \frac{d\Omega}{dr} \right) \left(\frac{-a}{p_0(0)} \frac{dp_0}{dr} \right) \right]^{\frac{1}{4}}. \quad (37)$$

It is again clear from this expression that unless both $\bar{\mu}$ and $\bar{\chi}_{\perp}$ are different from zero, the resistive interchange modes are linearly unstable for all m values.

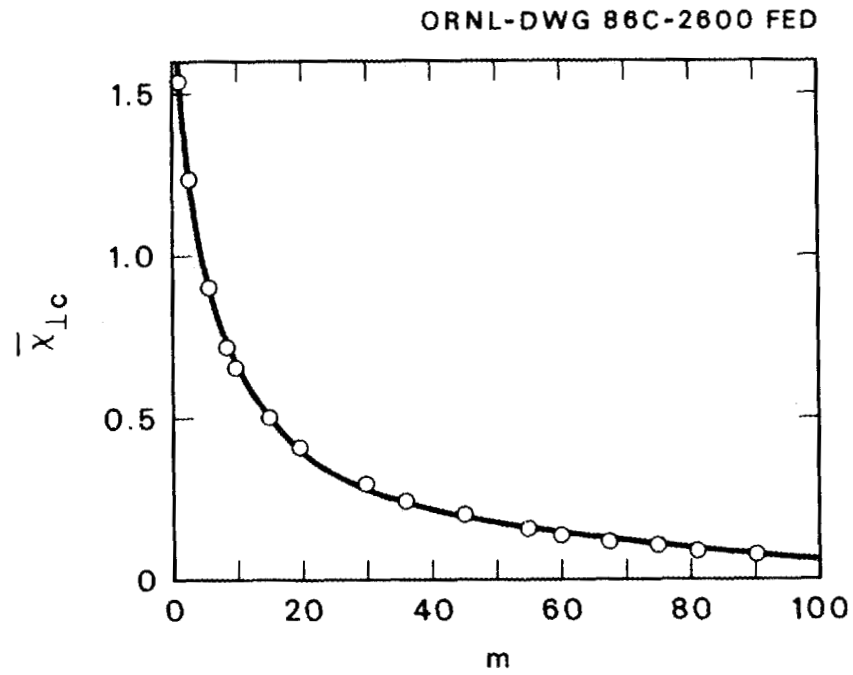


FIG. 2. Critical value of $\bar{\chi}_{\perp}$ for stabilization of the resistive interchange mode as a function of m .

IV. RENORMALIZED THEORY OF RESISTIVE PRESSURE-GRADIENT-DRIVEN TURBULENCE

In this section, the renormalized theory of resistive pressure-gradient-driven turbulence is presented. Renormalized response equations for resistive pressure-gradient-driven modes are derived. The consistency of the renormalized theory with constraints and conservation laws derived from the basic dynamical equations is discussed, and physical interpretations of the various nonlinear terms are proposed. A simplified set of renormalized equations that describe the dynamics of resistive pressure-gradient-driven modes is derived.

The simplest possible model of resistive pressure-gradient-driven turbulence is electrostatic and consists of the evolution equations for the vorticity U and pressure fluctuation \tilde{p} [Eqs. (8) and (9)]. In this model the equation for evolution of the kinetic energy, E_K , is

$$\frac{dE_K}{dt} = - \int \frac{dV}{\eta} \left(\nabla_{\parallel}^{(0)} \phi \right)^2 + \int dV V_r \tilde{p} \frac{d\Omega}{dr} - \mu \rho_m \int dV U^2 . \quad (38)$$

It differs from Eq. (14) in that the coupling to the magnetic energy appears as a resistive field line diffusion term. The pressure fluctuation equation (15) remains unchanged. In deriving Eqs. (15) and (38), the relations

$$\Delta E_K = \Delta E_p = 0 , \quad (39)$$

where

$$\Delta E_K = \int dV \phi (\nabla_{\perp} \phi \times \mathbf{z} \cdot \nabla_{\perp} U) \quad (40)$$

and

$$\Delta E_p = \int dV \tilde{p} (\nabla_{\perp} \phi \times \mathbf{z} \cdot \nabla_{\perp} \tilde{p}) , \quad (41)$$

were used. Equation (39) implies that although the nonlinearities of Eqs. (8) and (9) redistribute energy among various spatial scales, they do not enter the total energy balance of resistive pressure-gradient-driven turbulence. However, since the sources and sinks of energy act at disparate spatial scales, nonlinear energy transfer is required to achieve stationary turbulence.

As will be demonstrated, resistive fluid turbulence saturates by the mechanism of nonlinear transfer of energy from large to small scales. An analytical theory of such a process requires a renormalized two-point theory of the fluctuation spectrum to describe the nonlinear coupling of the region containing low- m energy to the large- m dissipation range. In the case when a few low- m modes dominate the energy spectrum, an alternative, more tractable calculation is to determine the energy outflow from the low- m modes required for saturation. Such a tactic is implemented by deriving low- m renormalized response equations and then determining the level of diffusion, representative of the spectrum-averaged rate of coupling to smaller scales, required for low- m saturation. The latter method is used for the study of resistive pressure-gradient-driven turbulence discussed in this paper.

Of course, this calculation of energy outflow from the low- m modes is meaningful only if there is sufficient large- m dissipation so that a saturated state is attainable. It is apparent from Eqs. (38) and (15) that dissipation in both the vorticity and pressure evolution equations is required for a nontrivial stationary state ($dp_0/dr \neq 0$). A related, but more subtle, requirement is that viscous dissipation and resistive diffusion are required in the vorticity evolution equation. The need for viscous dissipation is a consequence of the fact that nonlinear transfer to large- m modes ultimately couples to modes with m numbers for which $m/r > W_m^{(0)}$. Such m numbers correspond to modes in the fast interchange regime, with (ideal) growth rates given by Eq. (32), for which resistive field line diffusion is dynamically irrelevant. Thus, substantial viscous dissipation is required for the necessary stabilization of short-wavelength interchange modes.

Renormalized response equations, which describe the nonlinear dynamics of resistive pressure-gradient-driven modes in the presence of turbulence, are now derived. As in the linear calculation, a sheared-slab approximation is used, with

$y = r\theta$. Using a Fourier decomposition,

$$\begin{pmatrix} U \\ \phi \\ \tilde{p} \end{pmatrix} = \sum_{\mathbf{k}} \begin{pmatrix} U_{\mathbf{k}}(x, t) \\ \phi_{\mathbf{k}}(x, t) \\ \tilde{p}_{\mathbf{k}}(x, t) \end{pmatrix} \exp i(k_y y + k_z z) , \quad (42)$$

in Eqs. (8) and (9), we obtain

$$\frac{\partial U_{\mathbf{k}}}{\partial t} + N_{1\mathbf{k}} - \mu \nabla_{\perp}^2 U_{\mathbf{k}} = \frac{1}{\eta \rho_m} k_{\parallel}^2 \phi_{\mathbf{k}} - \frac{i}{\rho_m} \frac{d\Omega}{dr} k_y \tilde{p}_{\mathbf{k}} , \quad (43)$$

$$\frac{\partial \tilde{p}_{\mathbf{k}}}{\partial t} + N_{2\mathbf{k}} - \chi_{\perp} \nabla_{\perp}^2 \tilde{p}_{\mathbf{k}} = -i \frac{dp_0}{dr} k_y \phi_{\mathbf{k}} , \quad (44)$$

where $k_y \equiv m/r$, $k_z \equiv n/R_0$, and $k_{\parallel} = mB_0 x / (R_0 q L_q)$. The nonlinearities $N_{1\mathbf{k}}$ and $N_{2\mathbf{k}}$ are given by

$$\begin{aligned} N_{1\mathbf{k}} \equiv & \frac{\partial}{\partial x} \left[\sum_{\mathbf{k}'} (-ik'_y) (\phi_{-\mathbf{k}'} U_{\mathbf{k}''} - U_{-\mathbf{k}'} \phi_{\mathbf{k}''}) \right] \\ & - ik_y \left[\sum_{\mathbf{k}'} \left(\frac{\partial \phi_{-\mathbf{k}'}}{\partial x} U_{\mathbf{k}''} - \frac{\partial U_{-\mathbf{k}'}}{\partial x} \phi_{\mathbf{k}''} \right) \right] , \end{aligned} \quad (45)$$

$$\begin{aligned} N_{2\mathbf{k}} = & \frac{\partial}{\partial x} \left[\sum_{\mathbf{k}'} (-ik'_y) (\phi_{-\mathbf{k}'} \tilde{p}_{\mathbf{k}''} - \tilde{p}_{-\mathbf{k}'} \phi_{\mathbf{k}''}) \right] \\ & - ik_y \left[\sum_{\mathbf{k}'} \left(\frac{\partial \phi_{-\mathbf{k}'}}{\partial x} \tilde{p}_{\mathbf{k}''} - \frac{\partial \tilde{p}_{-\mathbf{k}'}}{\partial x} \phi_{\mathbf{k}''} \right) \right] . \end{aligned} \quad (46)$$

Here the wave vector $\mathbf{k}'' = \mathbf{k} + \mathbf{k}'$. The nonlinearities $N_{1\mathbf{k}}$ and $N_{2\mathbf{k}}$ are renormalized by iteratively substituting $U_{\mathbf{k}''}^{(2)}$, $\phi_{\mathbf{k}''}^{(2)}$ and $\tilde{p}_{\mathbf{k}''}^{(2)}$, fluctuations driven by the direct beat interaction of \mathbf{k} and \mathbf{k}' modes, for their corresponding factors in Eqs. (45) and (46).

The nonlinearly driven fluctuations are determined by

$$\Gamma_{1\mathbf{k}''} U_{\mathbf{k}''}^{(2)} - \frac{1}{\eta \rho_m} k_{\parallel}''^2 \phi_{\mathbf{k}''}^{(2)} + \frac{i}{\rho_m} \frac{d\Omega}{dr} k_y'' \tilde{p}_{\mathbf{k}''}^{(2)} = B_1 , \quad (47)$$

$$\Gamma_{2\mathbf{k}''} \tilde{p}_{\mathbf{k}''}^{(2)} + i \frac{dp_0}{dr} k_y'' \phi_{\mathbf{k}''}^{(2)} = B_2 , \quad (48)$$

where the propagators $\Gamma_{1\mathbf{k}''}$, $\Gamma_{2\mathbf{k}''}$ are

$$\Gamma_{1\mathbf{k}''} = \gamma_{\mathbf{k}''} + \Delta\omega_{\mathbf{k}''} - \mu \nabla_{\perp}^2 \quad (49)$$

$$\Gamma_{2\mathbf{k}''} = \gamma_{\mathbf{k}''} + \Delta\omega_{\mathbf{k}''} - \chi_{\perp} \nabla_{\perp}^2 \quad (50)$$

Here, $\gamma_{\mathbf{k}''}$ is the growth rate of the \mathbf{k}'' beat mode (which vanishes at saturation), and $\Delta\omega_{\mathbf{k}''}$ is the recursively defined decorrelation rate, which corresponds to the characteristic rate of nonlinear interaction for resistive pressure-gradient-driven turbulence. The beat-mode sources B_1 and B_2 are

$$B_1 = -ik'_y \phi_{\mathbf{k}'} \frac{\partial U_{\mathbf{k}}}{\partial x} + ik_y \frac{\partial \phi_{\mathbf{k}'}}{\partial x} U_{\mathbf{k}} - ik_y \phi_{\mathbf{k}} \frac{\partial U_{\mathbf{k}'}}{\partial x} + ik'_y \frac{\partial \phi_{\mathbf{k}}}{\partial x} U_{\mathbf{k}'} , \quad (51)$$

$$B_2 = -ik'_y \phi_{\mathbf{k}'} \frac{\partial \tilde{p}_{\mathbf{k}}}{\partial x} + ik_y \frac{\partial \phi_{\mathbf{k}'}}{\partial x} \tilde{p}_{\mathbf{k}} - ik_y \phi_{\mathbf{k}} \frac{\partial \tilde{p}_{\mathbf{k}'}}{\partial x} + ik'_y \frac{\partial \phi_{\mathbf{k}}}{\partial x} \tilde{p}_{\mathbf{k}'} . \quad (52)$$

Explicit calculation of the driven potential $\phi_{\mathbf{k}''}^{(2)}$ requires inversion of the eigenmode operator and results in complicated spatial convolution contributions to the renormalized response equations. Thus, it is worthwhile to consider possible simplifications of the renormalized theory. One such simplification follows from the observation that since resistive pressure-gradient-driven fluctuations are localized in radius, $N_{1\mathbf{k}'}$ can be expressed in terms of $U_{\mathbf{k}}^{(2)}$ alone. In particular, since

$$\sum_{\mathbf{k}'} = \sum_{m'} \sum_{n'} ,$$

it follows that, for a continuum of localized modes,

$$\sum_{\mathbf{k}'} = \int dm' \frac{|m'q'|}{q^2} \int dx' , \quad (53)$$

$$\frac{d}{dx'} = \frac{m}{m''} \frac{d}{dx''} . \quad (54)$$

Thus, an integration by parts in Eq. (45) yields

$$N_{1\mathbf{k}} = \frac{\partial}{\partial x} \left[\sum_{\mathbf{k}'} (-ik'_y) \phi_{-\mathbf{k}'} \left(\frac{m^2 + 2mm'}{m''^2} \right) U_{\mathbf{k}''}^{(2)} \right] - ik_y \left[\sum_{\mathbf{k}'} \frac{\partial \phi_{-\mathbf{k}'}}{\partial x} \left(\frac{m^2 + 2mm'}{m''^2} \right) U_{\mathbf{k}''}^{(2)} \right] . \quad (55)$$

Thus, since $N_{1\mathbf{k}}$ can be calculated using $U_{\mathbf{k}''}^{(2)}$ alone, and since $\phi_{\mathbf{k}''}^{(2)}$ contributions are spatially smooth in comparison to the more singular $U_{\mathbf{k}''}^{(2)}$, $\tilde{p}_{\mathbf{k}''}^{(2)}$ contributions, $\phi_{\mathbf{k}''}^{(2)}$ is hereafter neglected. It follows that

$$U_{\mathbf{k}''}^{(2)} = \frac{B_1}{\Gamma_{1\mathbf{k}''}} , \quad (56)$$

$$\tilde{p}_{\mathbf{k}''}^{(2)} = \frac{B_2}{\Gamma_{2\mathbf{k}''}} . \quad (57)$$

Finally, substitution of Eqs. (56) and (57) into Eqs. (45) and (46) yields

$$N_{1\mathbf{k}} = -\frac{\partial}{\partial x} \mu_{\mathbf{k}}^{xx} \frac{\partial}{\partial x} U_{\mathbf{k}} + k_y^2 \mu_{\mathbf{k}}^{yy} U_{\mathbf{k}} - \frac{\partial}{\partial x} C_{\mathbf{k}}^{xx} \frac{\partial}{\partial x} \phi_{\mathbf{k}} + k_y^2 C_{\mathbf{k}}^{yy} \phi_{\mathbf{k}} , \quad (58)$$

$$N_{2\mathbf{k}} = -\frac{\partial}{\partial x} D_{\mathbf{k}}^{xx} \frac{\partial}{\partial x} \tilde{p}_{\mathbf{k}} + k_y^2 D_{\mathbf{k}}^{yy} \tilde{p}_{\mathbf{k}} , \quad (59)$$

where

$$\mu_{\mathbf{k}}^{xx} = \sum_{\mathbf{k}'} \frac{m^2}{m''^2} k_y'^2 \langle \phi^2 \rangle_{\mathbf{k}'} \Gamma_{1\mathbf{k}''}^{-1} , \quad (60)$$

$$\mu_{\mathbf{k}}^{yy} = \sum_{\mathbf{k}'} \frac{m^2}{m''^2} \left\langle \left(\frac{\partial \phi}{\partial x} \right)^2 \right\rangle_{\mathbf{k}'} \Gamma_{1\mathbf{k}''}^{-1} , \quad (61)$$

$$C_{\mathbf{k}}^{xx} = \sum_{\mathbf{k}'} \frac{m^2}{m''^2} k_y'^2 \langle (\nabla'_{\perp} \phi)^2 \rangle_{\mathbf{k}'} \Gamma_{1\mathbf{k}''}^{-1} , \quad (62)$$

$$C_{\mathbf{k}}^{yy} = \sum_{\mathbf{k}'} \left(\frac{m}{m''} \right)^2 \left[\left\langle \left(\frac{\partial^2 \phi}{\partial x'^2} \right)^2 \right\rangle_{\mathbf{k}'} + k_y'^2 \left\langle \left(\frac{\partial \phi}{\partial x'} \right)^2 \right\rangle_{\mathbf{k}'} \right] \Gamma_{1\mathbf{k}''}^{-1} , \quad (63)$$

$$D_{\mathbf{k}}^{xx} = \sum_{\mathbf{k}'} k_y'^2 \langle \phi^2 \rangle_{\mathbf{k}'} \Gamma_{2\mathbf{k}''}^{-1} , \quad (64)$$

$$D_{\mathbf{k}}^{yy} = \sum_{\mathbf{k}'} \left\langle \left(\frac{\partial \phi}{\partial x'} \right)^2 \right\rangle_{\mathbf{k}'} \Gamma_{2\mathbf{k}''}^{-1} . \quad (65)$$

Here, terms of the form $\sum_{\mathbf{k}'} \phi_{-\mathbf{k}'} (\partial \phi_{\mathbf{k}'} / \partial x)$, etc., vanish due to symmetry considerations.

In order to gain physical insight into the structure of the renormalized response equations, it is useful to examine the consistency of the theory with the constraints

$\Delta E_K = \Delta E_p = 0$. In particular, using a local representation for brevity and clarity, ΔE_K and ΔE_p may be written as

$$\begin{aligned} \Delta E_K = & \sum_{\mathbf{k}, \mathbf{k}'} [\mathbf{k} \cdot (\mathbf{k}' \times \mathbf{z})] \left(\phi_{-\mathbf{k}} \phi_{-\mathbf{k}'} U_{\mathbf{k}''}^{(2)} - \phi_{-\mathbf{k}} U_{-\mathbf{k}'} \phi_{\mathbf{k}''}^{(2)} \right) \\ & - \sum_{\mathbf{q} + \mathbf{q}' = \mathbf{k}} [\mathbf{q} \cdot (\mathbf{q}' \times \mathbf{z})] \phi_{-\mathbf{q}} U_{-\mathbf{q}'} \phi_{\mathbf{q} + \mathbf{q}'}^{(2)} \end{aligned} \quad (66)$$

$$\begin{aligned} \Delta E_p = & \sum_{\mathbf{k}, \mathbf{k}'} [\mathbf{k} \times (\mathbf{k}' \times \mathbf{z})] \left(\tilde{p}_{-\mathbf{k}} \phi_{-\mathbf{k}'} \tilde{p}_{\mathbf{k}''}^{(2)} - \tilde{p}_{-\mathbf{k}} \tilde{p}_{-\mathbf{k}'} \phi_{\mathbf{k}''}^{(2)} \right) \\ & - \sum_{\mathbf{q} + \mathbf{q}' = \mathbf{k}} [\mathbf{q} \cdot (\mathbf{q}' \times \mathbf{z})] \tilde{p}_{-\mathbf{q}} \phi_{-\mathbf{q}'} \tilde{p}_{\mathbf{q} + \mathbf{q}'}^{(2)} . \end{aligned} \quad (67)$$

Thus, the renormalized theory preserves $\Delta E_K = 0$ via cancellation of coherent (\mathbf{k}) and incoherent (\mathbf{q}) mode coupling terms generated by $\phi_{\mathbf{k}''}^{(2)}$ interaction contributions, while $U_{\mathbf{k}''}^{(2)}$ contributions vanish by symmetry. Similarly, $\Delta E_p = 0$ is preserved by the cancellation of coherent and incoherent mode coupling terms generated by $\tilde{p}^{(2)}$ contributions, while $\phi_{\mathbf{k}''}^{(2)}$ contributions vanish by symmetry. Note that systematic application of the approximation $\phi_{\mathbf{k}''}^{(2)} = 0$ is consistent with the constraints $\Delta E_K = \Delta E_p = 0$. It follows that the renormalized response equations do not, and in fact cannot, conserve E_k and E_p . Indeed, the problem of the nonlinear interaction of a long-wavelength mode with turbulence is not one for which energy conservation is a crucial issue. However, the renormalized two-point theory can and must be consistent with energy conservation, as it is concerned with the nonlinear transfer of energy among different wave numbers.

A second noteworthy feature of the renormalized equations is the fact that $N_{1\mathbf{k}} \rightarrow 0$ as $m \rightarrow 0$. This is a consequence of direct relation of the vorticity U to the fluid that advects it. In particular, using a local representation it follows directly that

$$\begin{aligned} N_{1\mathbf{k}} = & \sum_{\mathbf{k}'} [\mathbf{k} \cdot (\mathbf{k}' \times \mathbf{z})] (\phi_{-\mathbf{k}'} U_{\mathbf{k}''} - U_{-\mathbf{k}'} \phi_{\mathbf{k}''}) \\ \cong & \sum_{\mathbf{k}'} [\mathbf{k} \cdot (\mathbf{k} \times \mathbf{z})] \left(\frac{\mathbf{k}_\perp^2 + 2\mathbf{k}_\perp \cdot \mathbf{k}'_\perp}{k''_\perp} \right) (\phi_{-\mathbf{k}'} U_{\mathbf{k}''}) . \end{aligned} \quad (68)$$

Thus, the $\mathbf{k} \rightarrow 0$ limit behavior of $N_{1\mathbf{k}}$ is a consequence of the competition between the reaction and the backreaction of the turbulent velocity field on the vorticity. Also, it is interesting to compare the structure of $N_{2\mathbf{k}}$ with $N_{1\mathbf{k}}$. In the latter case, since there is no simple link between \tilde{p} and ϕ , the representation of $N_{2\mathbf{k}}$ as the diffusion of a (nonlinearly) passive scalar \tilde{p} is possible.

Physical interpretations of the various terms of $N_{1\mathbf{k}}$ and $N_{2\mathbf{k}}$ are now proposed. Noting that, apart from the factor m^2/m''^2 induced by back reactions, $N_{1\mathbf{k}}$ is determined by energy-conserving $U_{\mathbf{k}}^{(2)}$ contributions, it follows that $\mu_{\mathbf{k}}^{xx}$ and $\mu_{\mathbf{k}}^{yy}$ correspond to (backreaction corrected) radial and poloidal diffusion of vorticity, that is, turbulent viscosity coefficients. Similarly, $C_{\mathbf{k}}^{yy}$ and $C_{\mathbf{k}}^{xx}$ conserve energy pairwise with $\mu_{\mathbf{k}}^{xx}$ and $\mu_{\mathbf{k}}^{yy}$, respectively. Indeed, note that while $\mu_{\mathbf{k}}^{xx}$ and $\mu_{\mathbf{k}}^{yy}$ are viscous energy sinks, $C_{\mathbf{k}}^{xx}$ and $C_{\mathbf{k}}^{yy}$ are destabilizing energy source counterterms. Finally, $D_{\mathbf{k}}^{xx}$ and $D_{\mathbf{k}}^{yy}$ correspond to radial and poloidal pressure diffusivities.

Further simplification of $N_{1\mathbf{k}}$ and $N_{2\mathbf{k}}$ is possible in the (interesting) limit of long wavelength, that is, for $|m| \ll \langle m^2 \rangle^{\frac{1}{2}}$, where $\langle m^2 \rangle$ refers to the rms poloidal mode number, defined according to

$$\langle m^2 \rangle = \sum_{\mathbf{k}} m^2 \langle \phi^2 \rangle_{\mathbf{k}} / \sum_{\mathbf{k}} \langle \phi^2 \rangle_{\mathbf{k}} . \quad (69)$$

In the long-wavelength limit $k_y W \ll 1$, and using the resistive layer width $W_m^{(0)}$ for W , $k_y W_m^{(0)} \sim k_y^{\frac{2}{3}}$. Thus, the spatial anisotropy of the spectrum is more pronounced at long wavelength. Hence, it follows that

$$-\frac{\partial}{\partial x} \mu_{\mathbf{k}}^{xx} \frac{\partial}{\partial x} U_{\mathbf{k}} \sim \frac{\langle m^2 \rangle}{r^2 W_m^{(0)2}} \alpha_{\mathbf{k}} , \quad (70)$$

$$k_y^2 \mu_{\mathbf{k}}^{yy} U_{\mathbf{k}} \sim \frac{m^2}{r^2 W_m^{(0)2} \overline{W}^2} \alpha_{\mathbf{k}} , \quad (71)$$

$$-\frac{\partial}{\partial x} C_{\mathbf{k}}^{xx} \frac{\partial \phi_{\mathbf{k}}}{\partial x} \sim \frac{m^2}{r^2 W_m^{(0)2} \overline{W}^2} \alpha_{\mathbf{k}} , \quad (72)$$

$$k_y^2 C_{\mathbf{k}}^{yy} \phi_{\mathbf{k}} \sim \frac{m^2}{r^2 \overline{W}^4} \alpha_{\mathbf{k}} , \quad (73)$$

where

$$\alpha_{\mathbf{k}} = \sum_{\mathbf{k}'} \left(\frac{m}{m''} \right)^2 \langle \phi^2 \rangle_{\mathbf{k}'} \Gamma_{1\mathbf{k}''}^{-1} \phi_{\mathbf{k}} \quad (74)$$

and \bar{W} is the mode width corresponding to $m = \langle m^2 \rangle^{\frac{1}{2}}$. Thus, since $m^2/(r^2 W_m^{(0)2}) < \langle m^2 \rangle/(r^2 \bar{W}^2)$, radial viscous diffusion [Eq. (70)] dominates poloidal diffusion [Eq. (71)] and its energy conserving counterterm $C_{\mathbf{k}}^{xx}$. Also, since $m^2/(r^2 \bar{W}^4) < \langle m^2 \rangle/(r^2 W_m^{(0)4})$ for $m < \langle m^2 \rangle$, the term in Eq. (73) is also negligible. Finally, for similar reasons,

$$\left\| -\frac{\partial}{\partial x} D_{\mathbf{k}}^{xx} \frac{\partial \tilde{p}_{\mathbf{k}}}{\partial x} \right\| \gg \|k_y^2 D_{\mathbf{k}}^{yy} \tilde{p}_{\mathbf{k}}\| . \quad (75)$$

The validity and accuracy of these approximations have been studied and confirmed using the results of the numerical calculations.

Having exploited the possibilities for simplification in the limit where $m < \langle m^2 \rangle^{\frac{1}{2}}$, we find that the renormalized response equations for stationary, long-wavelength resistive interchange modes are

$$\mu \nabla_{\perp}^2 U_{\mathbf{k}} - \nabla_{\perp} \mu_{xx} \cdot \nabla_{\perp} U_{\mathbf{k}} = \frac{1}{\eta \rho_m} k_{\parallel}^2 \phi_{\mathbf{k}} - \frac{i}{\rho_m} \frac{d\Omega}{dr} k_y \tilde{p}_{\mathbf{k}} , \quad (76)$$

$$-\chi_{\perp} \nabla_{\perp}^2 \tilde{p}_{\mathbf{k}} - \nabla_{\perp} D_{xx} \nabla_{\perp} \tilde{p}_{\mathbf{k}} = -i \frac{dp_0}{dr} k_y \phi_{\mathbf{k}} , \quad (77)$$

where

$$D_{xx} = \sum_{m', n'} \left(\frac{m'}{r} \right)^2 \langle \phi^2 \rangle_{\mathbf{k}'} \Gamma_{2\mathbf{k}'}^{-1} , \quad (78)$$

$$\mu_{xx} = \sum_{m', n'} \left(\frac{m}{m''} \right)^2 \left(\frac{m'}{r} \right)^2 \langle \phi^2 \rangle_{\mathbf{k}'} \Gamma_{1\mathbf{k}''}^{-1} . \quad (79)$$

In the following section, the nonlinear diffusivities D_{xx} and μ_{xx} at saturation will be obtained by solving Eqs. (76) and (77), assuming a relationship between μ_{xx} and D_{xx} and treating D_{xx} as the eigenvalue to be determined.

V. SOLUTION OF THE RENORMALIZED EQUATIONS FOR THE RESISTIVE PRESSURE-GRADIENT-DRIVEN TURBULENCE

In this section, an analytic solution to the renormalized equations is determined. This solution gives the necessary level of diffusion induced by the resistive pressure-gradient-driven turbulence required for saturation. From this result, the saturation level of the turbulence can be estimated.

The renormalized equations derived in Sec. IV generalize previous results,⁷ but their structure is not essentially different. The most important results of the present paper, which differ from previous results, arise from the way the saturation condition is defined. In previous calculations, the condition for saturated turbulence was established by balancing the $\partial\tilde{p}/\partial t$ term with the nonlinear diffusion term for the lowest m unstable mode.^{3,4,6} This leads to the mixing length result

$$D_{xx} \sim \gamma_m^{(0)} W_m^{(0)2} . \quad (80)$$

This result can also be derived from the invariance condition on the basic set of equations,⁵ Eqs. (1)–(3), for the case $\mu = \chi_{\perp} = 0$.

Here, an accurate saturation condition is imposed by setting all time derivatives equal to zero. This definition is valid only if dissipation terms are included in the equations, so that they balance driving terms. The form of the renormalized equations is very similar to that of the linear stability equations. Therefore, the renormalized equations can be written in a dimensionless form by performing a change of variables analogous to that in Sec. III. We obtain

$$\frac{d^4 \Phi_m}{dX^4} - 2 \frac{d^2 \Phi_m}{dX^2} + \Phi_m = AP_m + BX^2 \Phi_m , \quad (81)$$

$$\frac{d^2 P_m}{dX^2} = P_m + \Phi_m , \quad (82)$$

with

$$A = \left[\frac{\beta_0}{2\epsilon^2} \left(a \frac{d\Omega}{dr} \right) \left(\frac{-a}{p_0(0)} \frac{dp_0}{dr} \right) \right] \left(\frac{r}{am} \right)^4 \frac{a^4 S^2}{\tau_R^2 (D_{xx} + \chi_{\perp}) (\mu_{xx} + \mu)} , \quad (83)$$

$$B = m^2 \left(\frac{a^2 \mu_0}{\tau_R \eta} \right) \left(\frac{r}{am} \right)^6 S^2 \left(\frac{a}{qL_q} \right)^2 \frac{a^2}{\tau_R (\mu_{xx} + \mu)} . \quad (84)$$

Note that

$$\frac{A}{B} = \frac{\gamma_m^{(0)} W_m^{(0)2}}{D_{xx} + \chi_{\perp}} . \quad (85)$$

Assuming that there is a known relationship between μ_{xx} and D_{xx} , Eqs. (81) and (82) define an eigenvalue problem, the solution of which gives a relationship between A and B . That is, $A = F(B)$ where F is the function to be found by solving the eigenvalue problem. Such a relation implies that

$$D_{xx} + \chi_{\perp} = \gamma_m^{(0)} W_m^{(0)2} \hat{F}(B) , \quad (86)$$

where $\hat{F}(B) = B/F(B)$. This expression shows that a correction factor, weakly dependent on β and the driving terms, multiplies the mixing length result. We can explicitly calculate this factor in some relevant limits. In particular, for high S and low m , we can proceed to solve the eigenvalue problem, Eqs. (81) and (82), in the same way as the linear problem. This limit is probably the most relevant one for applications to magnetically confined plasmas. By carrying out the same type of calculation as in Sec. III, we can derive an equation analogous to Eq. (34),

$$D_{xx} + \chi_{\perp} = \gamma_m^{(0)} W_m^{(0)2} \left\{ \frac{2}{3\pi} \ln \left[\frac{64a^4 K_1}{\tau_R^2 (D_{xx} + \chi_{\perp}) (\mu_{xx} + \mu)} \right] \right\}^2 , \quad (87)$$

where K_1 is given by Eq. (24). From this expression, it is clear that if the collisional dissipation is small in comparison to the turbulence-induced diffusion, which is in general the case for the low- m modes ($\mu \ll \mu_{xx}$ and $\chi_{\perp} \ll D_{xx}$), we can neglect χ_{\perp} and μ . This means that for low- m modes the level of nonlinear dissipation necessary for stationary resistive pressure-gradient-driven turbulence is independent of the collisional dissipation. It is important to note that no saturation is possible if the collisional dissipation is zero. The collisional dissipation is needed to produce a sink of energy at high m and thus provide a stabilization mechanism for the high- m fluctuations. As the spectrum of fluctuation is dominated by the low- m modes and D_{xx} is large for these m values, the level of saturation is not so sensitive to the dissipation parameters.

The following are the main properties of the nonlinear diffusion coefficient D_{xx} :

- (1) The scaling with β is very close to linear, as in the mixing length prediction (Fig. 3).
- (2) For realistic values of the dissipation coefficients, the size of D_{xx} is about an order of magnitude larger than the mixing length result (Fig. 3).
- (3) The correction factor gives a weak dependence on m , close to m^{-1} , but the validity of Eq. (87) is limited to the low- m range.
- (4) The dependence on μ and χ_{\perp} is weak (Fig. 3) for realistic values of these parameters.

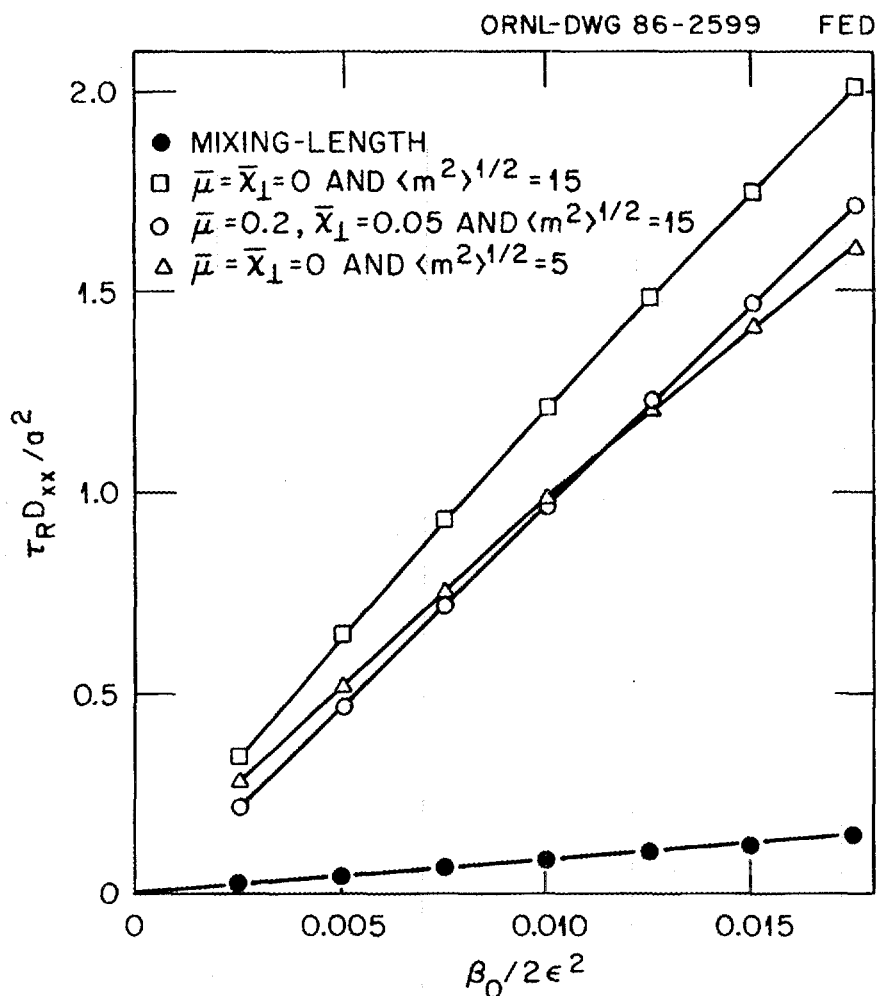


FIG. 3. Scaling of the nonlinear diffusion coefficient D_{xx} with $\beta_0/2\epsilon^2$, for different values of the dissipation coefficients. The value of D_{xx} calculated using Eq. (87) is compared with the mixing length prediction.

Once the relation between the coefficients D_{xx} and μ_{xx} is known, we can go further and estimate the turbulence level at saturation. This calculation requires further assumptions. First, we can estimate the decorrelation rate in the propagators, Eqs. (49) and (50), in the following way:

$$\Gamma_1 \cong \frac{\mu_{xx}}{\Delta_m^2} , \quad (88)$$

$$\Gamma_2 \cong \frac{D_{xx}}{\delta_m^2} . \quad (89)$$

Here Δ_m and δ_m are the characteristic scale lengths of the potential and pressure fluctuations respectively. Using Eqs. (78) and (79), we can find a relation between the μ_{xx} and D_{xx} coefficients,

$$\mu_{xx} \cong \frac{m^2}{\langle m^2 \rangle} \frac{\Delta_{\langle m \rangle}}{\delta_{\langle m \rangle}} D_{xx} . \quad (90)$$

Similarly, we estimate the mean-square turbulent radial velocity,

$$\langle \tilde{V}_r^2 \rangle \cong D_{xx}^2 / \delta_{\langle m \rangle}^2 . \quad (91)$$

It is now necessary to evaluate the two basic nonlinear scale lengths appearing in Eqs. (90) and (91). The nonlinear width Δ_m of the radial velocity fluctuations can be estimated by balancing the viscosity term with the field line bending term. This yields

$$\Delta_m = \frac{1}{m^{\frac{1}{5}}} \left(\frac{\tau_R \mu_{xx}}{a^2} \frac{\tau_R \eta}{a^2 \mu_0} \right)^{\frac{1}{6}} \frac{1}{S^{\frac{1}{5}}} \left(\frac{qLq}{a} \right)^{\frac{1}{5}} a . \quad (92)$$

The pressure fluctuation level and its nonlinear width can be evaluated from two other relations: first, balancing the nonlinear diffusion with the driving term in the pressure equation; second, and for $x \approx 0$, balancing the curvature term with the nonlinear viscosity term in the momentum balance equation. This yields the two relations

$$\langle \tilde{p}^2 \rangle^{\frac{1}{2}} \cong \left| \frac{dp_0}{dr} \right| \frac{\delta_{\langle m \rangle}^2}{D_{xx}} \langle \tilde{V}_r^2 \rangle^{\frac{1}{2}} , \quad (93)$$

$$\begin{aligned} \Delta_{\langle m \rangle} \delta_{\langle m \rangle} &\cong \left[\frac{\beta_0}{2\epsilon^2} \left(a \frac{d\Omega}{dr} \right) \left(\frac{-a}{p_0(0)} \frac{dp_0}{dr} \right) \right]^{-\frac{1}{3}} \\ &\times S^{-\frac{2}{3}} \left(\frac{\tau_R D_{xx}}{a^2} \right)^{\frac{2}{3}} \left(\frac{r_s^2}{a^2 \langle m^2 \rangle} \right)^{\frac{1}{3}} a^2 . \end{aligned} \quad (94)$$

Using Eqs. (90)–(94), one obtains an estimate for all the physics parameters relevant to resistive pressure-gradient-driven turbulence. They are

$$\Delta_m \cong W_m^{(0)} \Lambda^{\frac{1}{6}} , \quad (95)$$

$$\delta_m \cong W_m^{(0)} \Lambda^{\frac{7}{6}} , \quad (96)$$

$$\langle \tilde{V}_r^2 \rangle^{\frac{1}{2}} \cong \gamma_{\langle m \rangle}^{(0)} W_{\langle m \rangle}^{(0)} \Lambda^{\frac{5}{6}} , \quad (97)$$

$$\langle \tilde{p}^2 \rangle^{\frac{1}{2}} \cong \left| \frac{dp_0}{dr} \right| W_{\langle m \rangle}^{(0)} \Lambda^{\frac{7}{6}} , \quad (98)$$

$$D_{xx} \cong \gamma_{\langle m \rangle}^{(0)} \left(W_{\langle m \rangle}^{(0)} \right)^2 \Lambda^2 , \quad (99)$$

$$\mu_{xx} \cong \frac{m^2}{\langle m \rangle} \gamma_{\langle m \rangle}^{(0)} \left(W_{\langle m \rangle}^{(0)} \right)^2 \Lambda , \quad (100)$$

where

$$\Lambda \equiv \frac{2}{3\pi} \ln \left[\frac{\beta_0}{\epsilon^2} \left(a \frac{d\Omega}{dr} \right) \left(\frac{-a}{p_0(0)} \frac{dp_0}{dr} \right) \left(\frac{r}{am_0} \right)^4 \frac{64a^4 S^2}{\tau_R^2 D_{xx} \mu_{xx}} \right] . \quad (101)$$

The results shown in Eqs. (95)–(100) are those expected from mixing length theory multiplied by the enhancement factor Λ to a power. For realistic parameters, $\Lambda > 1$. Therefore, the previous relations imply that the pressure fluctuation scale length is larger than that of the velocity fluctuations, $\delta_m > \Delta_m$. The nonlinearly induced pressure diffusion coefficient is also larger than the nonlinearly induced viscosity, and the predicted fluctuation levels are higher than the mixing length theory predictions.

VI. THREE-DIMENSIONAL NUMERICAL CALCULATIONS OF RESISTIVE PRESSURE-GRADIENT-DRIVEN TURBULENCE

In this section, the results of the three-dimensional numerical calculations are presented. It is shown that a state of stationary turbulence in the presence of a nonzero average pressure gradient is attained. The effects of collisional dissipation are discussed and the scaling of the saturation levels is presented.

The numerical calculations have been performed using equilibrium parameters relevant to stellarator devices. However, the basic model used in this paper has been simplified to maximize the understanding of the dynamical mechanisms. The numerical results are not intended to be a simulation of a stellarator plasma. The rotational transform has been parametrized as

$$\iota(r) = 0.53 + 0.50 \left(\frac{r^2}{a} \right)^2, \quad (102)$$

and Ω is such that a localized region of bad curvature ($0.35 \leq r/a \leq 0.65$) exists away from the wall. With this choice of parameters, the unstable region exists for values of the transform $0.59 \leq \iota \leq 0.75$. The lowest m resonant mode is the ($m = 3; n = 2$) mode. At the resonant surface of this mode, the physical parameters are those given in Table I. The main reason for restricting the unstable region to one-third of the plasma minor radius is to maximize resolution in the numerical calculations. The pressure profile chosen is $p_0(r) = p_0(0) \left(\psi(r)/\psi(0) \right)^2$, and the expression for the poloidal flux ψ can be calculated from Eq. (92). For these equilibrium parameters, the threshold for ideal pressure-driven instabilities is at $\beta_0/2\epsilon^2 = 0.037$ (Fig. 4). In this paper, the nonlinear calculations for resistive pressure-driven instabilities have been performed for values of β well below the ideal threshold. The highest β value considered is $\beta_0/2\epsilon^2 = 0.0125$, and β has been varied between this upper limit and $\beta_0/2\epsilon^2 = 0.0025$. For these different β values the dissipation coefficients $\bar{\mu}$ and $\bar{\chi}_\perp$ have been chosen in such a way that the linearly unstable mode with the shortest wavelength had an m value below 70 (Fig. 5). This restriction is due to the number of modes that can be retained in the

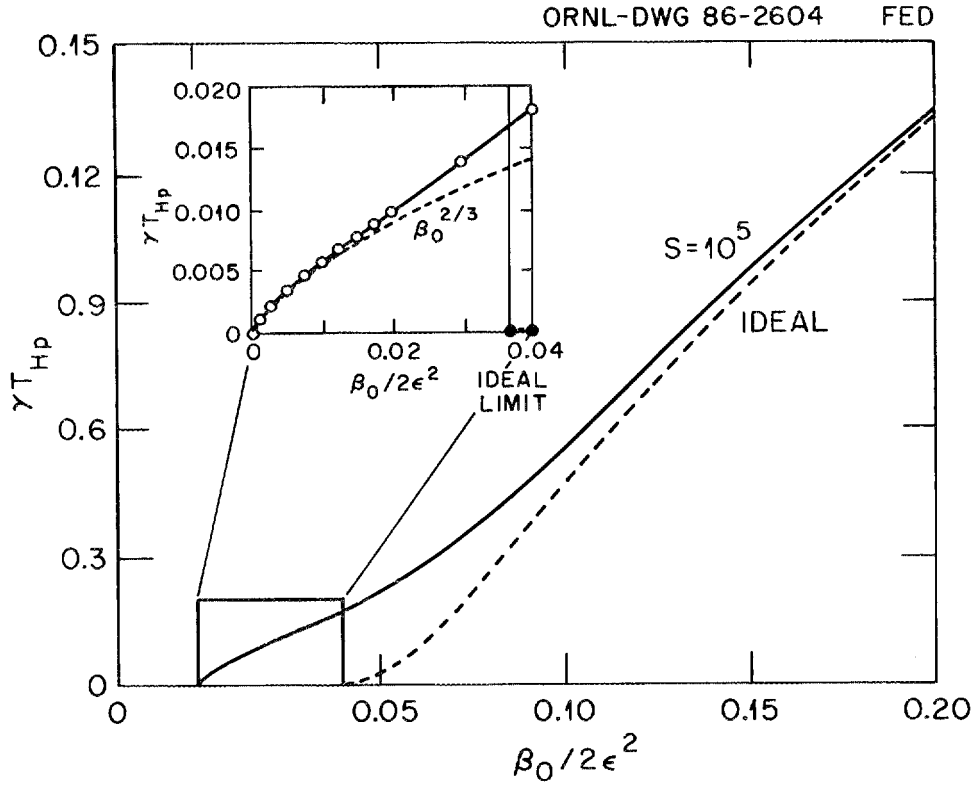


FIG. 4. Linear growth rate of the ($m = 3$; $n = 2$) interchange mode as a function of $\beta_0/2\epsilon^2$, comparing the resistive ($S = 10^5$) and the ideal ($S = \infty$) growth rates.

nonlinear numerical calculations, which is limited to 800. Table II gives the values of these parameters used for the present calculations. The S value has been set at $S = 10^5$ for all the calculations presented here.

The three-dimensional nonlinear calculations have been done using the KITE code,¹² an initial value code that solves Eqs. (1)–(3) using a Fourier expansion in the angles θ and $\zeta \equiv z/R_0$ and finite differences in the radial variable. For details of the numerical scheme, see Ref. 11. For the present calculations, radial grid spacings $\Delta r = 2.4 \times 10^{-3}$ have been routinely used. Convergence has been tested by varying the Δr grid spacing up to $\Delta r = 1.2 \times 10^{-3}$. With this grid, even the highest m modes included in the calculation are well resolved. The number of Fourier components

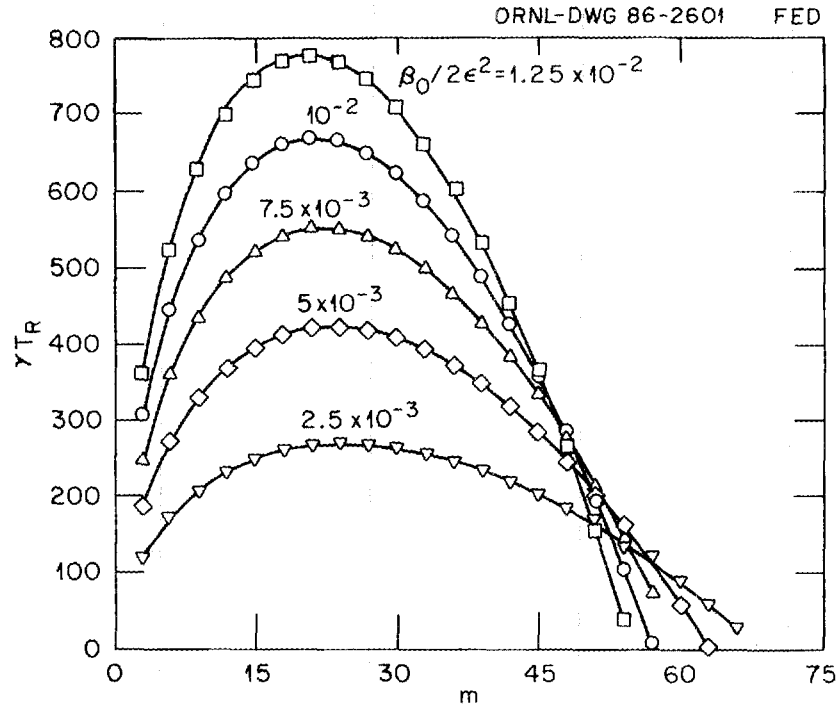


FIG. 5. Linear growth rate vs m of the resistive interchange mode for the different equilibrium parameters given in Table II.

Table II. Parameters used in the nonlinear numerical calculations discussed in Sec. VI together with the obtained rms values of m and the corresponding dominant m_0 value

$\beta_0/2\epsilon^2$	$\bar{\mu}$	$\bar{\chi}_\perp$	m_0	$\langle m^2 \rangle^{\frac{1}{2}}$
0.0025	0.0294	0.008	12	11.7 ± 0.3
0.0050	0.0676	0.0175	6	8.8 ± 1.4
0.0075	0.110	0.0275	3	4.0 ± 0.4
0.0100	0.154	0.0385	3	4.7 ± 0.6
0.0125	0.20	0.050	3	4.6 ± 0.7

used for most calculations has been 244 or 548. For convergence testing, up to 750 modes have been used. In all the calculations discussed here, the modes included in the calculation were all initialized at the same amplitude.

Let us consider the case with $\beta_0/2\epsilon^2 = 0.0125$ as a paradigm and discuss the main features of the time evolution of the instabilities. It is important first to point out that if the modes included in the nonlinear calculation are all linearly unstable, then no steady-state solution is ever reached. This is, of course, logical, because in such cases there is no sink of energy to balance the instability-driving terms. This situation is equivalent to the zero dissipation case. As more Fourier components are added to the calculation and the range of linearly stable modes is increased, the fluctuations saturate at a finite level (Fig. 6). In this particular case, about 244 modes are enough to give a converged solution. When 548 modes are included, the same level of fluctuations is reached. This convergence must be understood in a time-averaged sense. The results shown in Fig. 7 were obtained with $\bar{\mu} = 0.2$ and $\bar{\chi}_\perp = 0.05$. Increasing these parameters to $\bar{\mu} = 0.26$ and $\bar{\chi}_\perp = 0.065$ did not change the saturated level of the fluctuations. Furthermore, while the role of the dissipation is important for producing a high- m energy sink, it should weakly affect the low- m saturation level. This was tested by excluding the viscosity and cross-field transport ($\bar{\mu} = 0$ and $\bar{\chi}_\perp = 0$) for all components with $m < 12$. The time evolution changes (Fig. 7) because the linear growth rates of the $m < 12$ modes are affected by the dissipative terms (Fig. 1b). However, the saturation level of the fluctuations reached is the same as in the case with $\bar{\mu} \neq 0$ and $\bar{\chi}_\perp \neq 0$ for all modes.

In the numerical calculations, the pressure equation includes a term that is not present in Eq. (3). The pressure equation is written as

$$\frac{\partial \tilde{p}}{\partial t} = -V_r \frac{dp_0}{dr} + \chi_\perp \nabla_\perp^2 \tilde{p} + \chi_\parallel \nabla_\parallel^2 \tilde{p} . \quad (103)$$

The last term in Eq. (103) has been included to control the width of the pressure fluctuation in the nonlinear evolution. In the calculation, the value for χ_\parallel is chosen

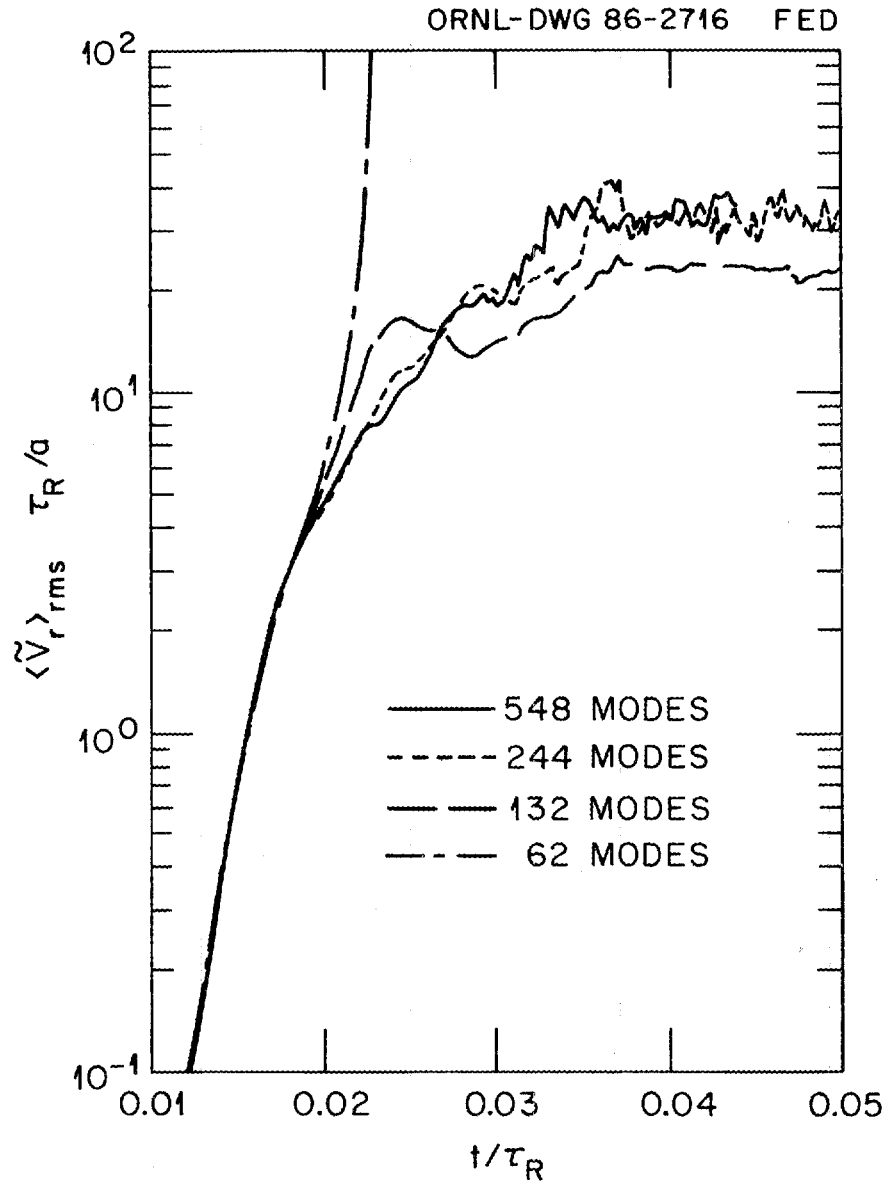


FIG. 6. Nonlinear evolution of $\langle \tilde{V}_r^2 \rangle^{1/2}$ for the $\beta_0/2\epsilon^2 = 0.0125$ case, comparing the different sets of modes included in the calculation.

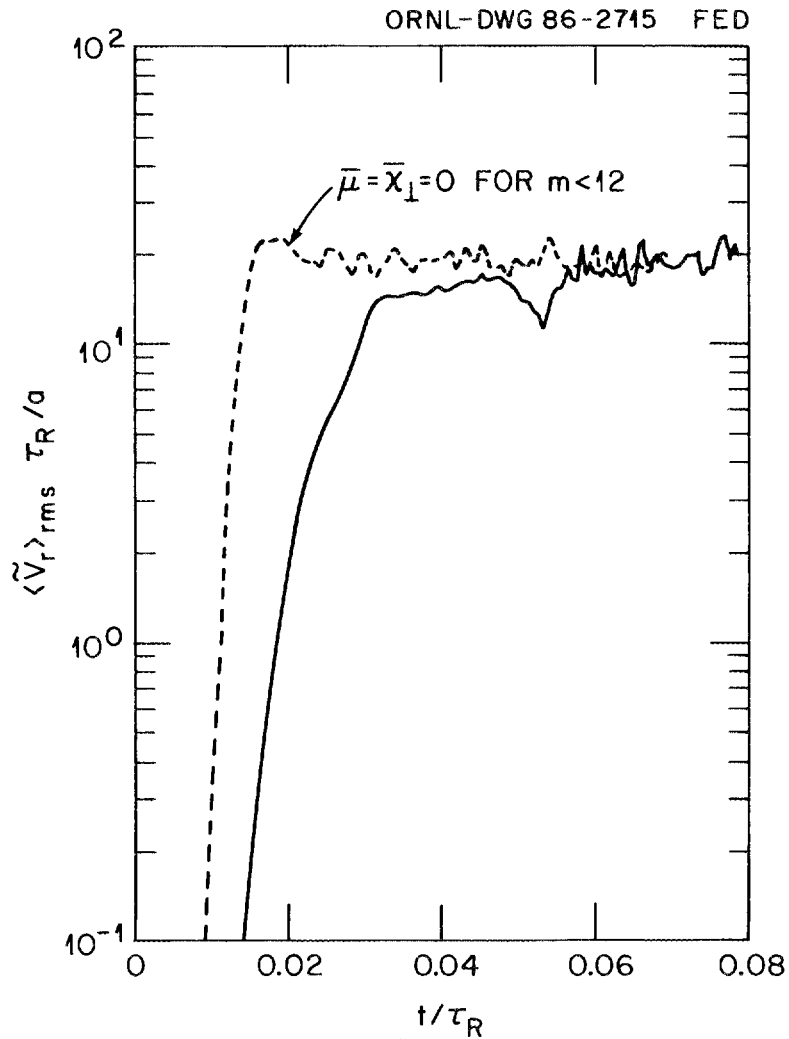


FIG. 7. Nonlinear evolution of $\langle \tilde{V}_r^2 \rangle^{\frac{1}{2}}$ for the $\beta_0/2\epsilon^2 = 0.010$ case, showing the effect of eliminating the collisional dissipation terms for the low- m ($m < 12$) modes.

so that it does not change the radial width of the low- m linear eigenfunctions. The value $\chi_{||} = 10^5 R_0^2 / \tau_R$ is used in most of the calculations. This value has been varied by two orders of magnitude, weakly affecting the saturation level of the velocity fluctuation. Table III gives the rms values of the radial velocity, pressure, and potential fluctuations resulting from these calculations. The value of β is $\beta_0/2\epsilon^2 = 0.01$, and $S = 10^5$. The values are time averaged over the steady-state

Table III. Effect of χ_{\parallel} on the saturation level of the resistive pressure-gradient-driven turbulence

$\chi_{\parallel} R_0^2 / \tau_R$	$(\tilde{V}_r)_{\text{rms peak}}$	$\langle m^2 \rangle^{\frac{1}{2}}$	$(\tilde{p})_{\text{rms peak}}$	$(\tilde{\phi})_{\text{rms peak}}$
10^3	115 ± 23	5.5 ± 0.9	0.118 ± 0.016	3.2 ± 1.2
10^4	110 ± 12	4.9 ± 0.8	0.117 ± 0.012	3.5 ± 1.2
10^5	96 ± 23	4.7 ± 0.6	$(8.5 \pm 0.9)10^{-2}$	2.9 ± 0.6

period, and the errors are based on the standard deviation over these mean values. The effect of χ_{\parallel} is more important for the very low m modes because of their large nonlinear widths. The contribution of the lowest m mode has not been included in the values given in Table III. Therefore, it is clear that the χ_{\parallel} term in Eq. (103) does not strongly affect the dynamical evolution of the resistive pressure-gradient-driven turbulence for the range of values considered in these calculations.

It is clear that the χ_{\parallel} effect is important in the nonlinear regime only when $\delta_m \sim \Delta_{\parallel}$. Here Δ_{\parallel} is the characteristic length associated with the χ_{\parallel} term and is given by

$$\Delta_{\parallel} = \left(\frac{\tau_R D_{xx}}{a^2} \right)^{\frac{1}{4}} \left(\frac{\tau_R \chi_{\parallel}}{R_0^2} \right)^{-\frac{1}{4}} \left(\frac{q L_q}{m a} \right)^{\frac{1}{2}} a. \quad (104)$$

Therefore, χ_{\parallel} must fulfill the condition

$$\chi_{\parallel} < \left(\frac{a}{m r_s} \right)^{\frac{2}{3}} \left[\frac{\beta_0}{2\epsilon^2} \left(a \frac{d\Omega}{dr} \right) \left(\frac{-a}{p_0(0)} \frac{dp_0}{dr} \right) \right]^{\frac{1}{3}} \left(\frac{\tau_R \eta}{a^2 \mu_0} \right)^{-\frac{1}{3}} \\ \times \left[\frac{2}{3\pi} \ln \left(64 \frac{a^4 K_1}{\tau_R^2 D_{xx} \mu_{xx}} \right) \right]^{-\frac{8}{3}} S^{\frac{4}{3}} \left(\frac{q^2 L_q^2}{a^2} \right)^{\frac{8}{3}} \frac{R_0^2}{\tau_R} \quad (105)$$

to avoid affecting the dynamical evolution of the pressure-gradient-driven turbulence.

The nonlinear stability of a sequence of equilibria with different values of $\beta_0/2\epsilon^2$ has been numerically studied (see Table II). The values of the V_r and \tilde{p} fluctuations at saturation are given in Fig. 8. These values have been calculated by averaging the local values at $r_s = 0.523a$ over time. The error bar corresponds to one standard deviation. The solid points are the analytical results, calculated with Eqs. (97) and (98). The values for $\langle m^2 \rangle$ used in these equations are those from the numerical results. The scaling with β is very well reproduced by the analytical model, and the agreement shown in Fig. 8 is good. The importance of the logarithmic factor in modifying the mixing length is clear. At the lowest β value ($\beta_0/2\epsilon^2 = 0.0025$), the mixing length prediction for (\tilde{V}_r^2) is a factor of 4.5 smaller than that given by Eq. (97). At the highest β value ($\beta_0/2\epsilon^2 = 0.0125$), the factor is 8.5.

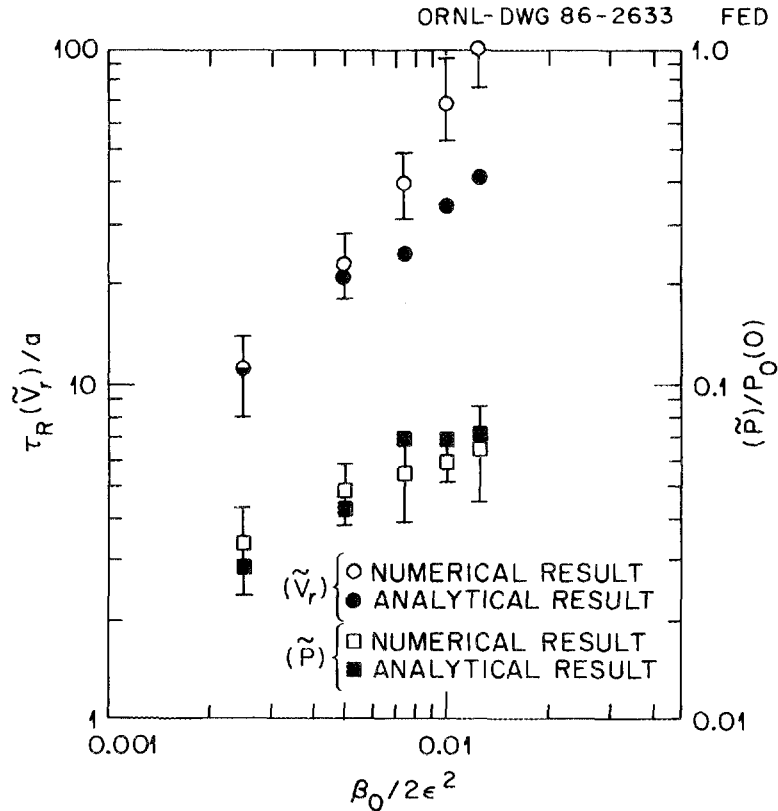


FIG. 8. Comparison of the analytical and numerical results for the fluctuation levels of the resistive pressure-gradient-driven turbulence.

The pressure diffusion coefficient has also been calculated from the numerical results, using the expression

$$D = \left| \frac{dp_0}{dr} \right|^{-1} \langle \tilde{V}_r \tilde{p} \rangle . \quad (106)$$

The analytic prediction, Eq. (99), agrees well with the numerical results (Fig. 9). The analytic result gives the correct β scaling and magnitude. The discrepancy from the mixing length prediction is quite clearly shown in the figure.

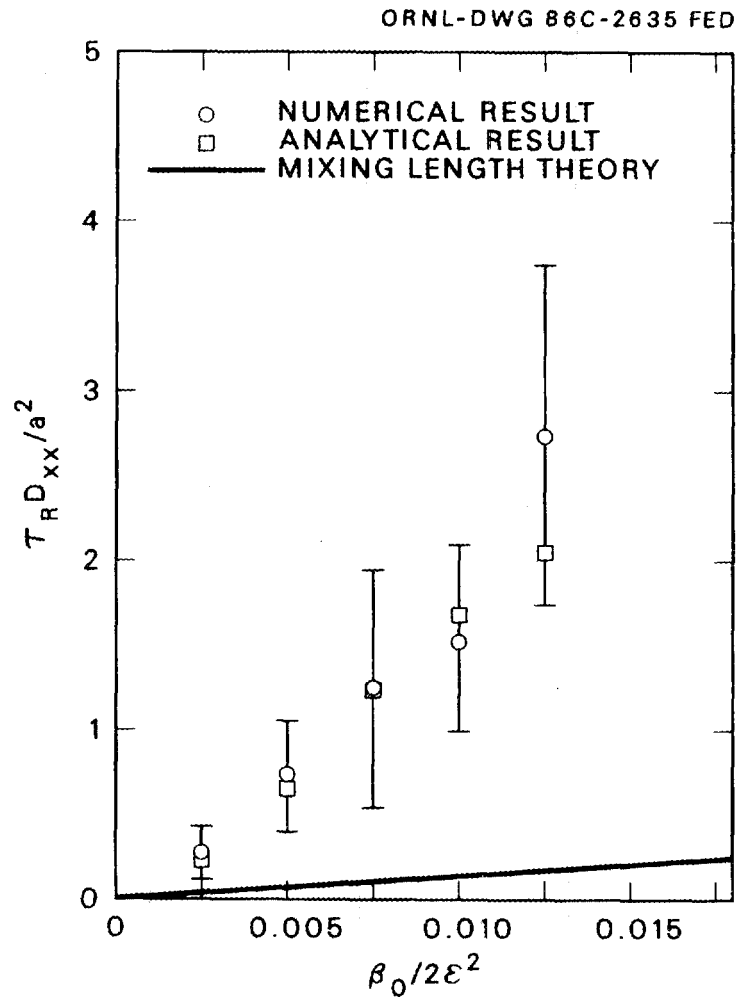


FIG. 9. Comparison of the analytical and numerical results for the nonlinear diffusion coefficient. Both show clear discrepancy from the mixing length predictions.

VII. CONCLUSIONS

Detailed study of resistive pressure-gradient-driven turbulence using a simple model has unveiled some new and interesting features of the dynamics of these problems. The main results obtained are as follows.

- (1) The linear stability of resistive interchange modes with viscosity and thermal diffusivity has been studied, and the existence of a range of stable large- m modes has been demonstrated.
- (2) The existence of well-converged, saturated turbulent states with fixed pressure gradient has been demonstrated using the numerical calculations.
- (3) A well-defined saturation criterion is proposed, and a renormalized theory of resistive pressure-gradient-driven turbulence is presented. The predicted pressure diffusivity at saturation is

$$\begin{aligned}
 D_{xx} &= \gamma_m^{(0)} W_m^{(0)2} \left[\frac{2}{3\pi} \ln \left(\frac{64a^4 K_1}{\tau_R^2 D_{xx} \mu_{xx}} \right) \right]^2 \\
 &= \frac{\beta_0}{2\epsilon^2} \left(a \frac{d\Omega}{dr} \right) \left(\frac{-a}{p_0(0)} \frac{dp_0}{dr} \right) \left(\frac{qL_q}{r} \right)^2 \frac{\tau_R \eta}{a^2 \mu_0} \\
 &\quad \times \left\{ \frac{2}{3\pi} \ln \left[\frac{\beta_0}{\epsilon^2} \left(a \frac{d\Omega}{dr} \right) \left(\frac{-a}{p_0(0)} \frac{dp_0}{dr} \right) \left(\frac{r}{am} \right)^4 \frac{64a^4 S^2}{\tau_R^2 \mu_{xx} D_{xx}} \right] \right\}^2. \quad (107)
 \end{aligned}$$

The results of the numerical calculations are in good agreement with theoretical predictions.

- (4) While the leading parameter scaling of D_{xx} agrees with the simple mixing length predictions, significant quantitative enhancement and additional parameter dependence are predicted. The enhancement effects over the simple mixing length predictions can have important implications for the previously derived transport coefficients.³⁻⁶ To discuss these implications, it is necessary to use a more realistic model and consider the effects of the magnetic fluctuations. This is beyond the scope of this paper. However, modifications comparable to those discussed here would probably carry over. This could imply transport enhancement up to one order of magnitude over previous results.

ACKNOWLEDGMENT

The authors would like to acknowledge G. S. Lee for many useful discussions and for his comments on the manuscript.

REFERENCES

- ¹ H. P. Furth, J. Killeen, and M. N. Rosenbluth, *Phys. Fluids* **6**, 77 (1963).
- ² B. Coppi, *Phys. Fluids* **7**, 1501 (1964).
- ³ K. C. Shaing and B. A. Carreras, *Phys. Fluids* **28**, 2027 (1985).
- ⁴ Z. G. An, P. H. Diamond, R. D. Hazeltine, J. N. Leboeuf, M. N. Rosenbluth, R. D. Sydora, T. Tajima, B. A. Carreras, L. Garcia, T. C. Hender, H. R. Hicks, J. A. Holmes, V. E. Lynch, and H. R. Strauss, *Plasma Physics and Controlled Nuclear Fusion Research, Tenth International Conference, London* (IAEA, Vienna, 1985), Vol. 2, p. 231.
- ⁵ J. W. Connor and J. B. Taylor, in *Plasma Physics and Controlled Nuclear Fusion Research, Tenth International Conference, London* (IAEA, Vienna, 1985), Vol. 2, p. 13.
- ⁶ B. A. Carreras, P. H. Diamond, M. Murakami, J. L. Dunlap, J. D. Bell, H. R. Hicks, J. A. Holmes, E. A. Lazarus, V. K. Paré, P. Similon, C. E. Thomas, and R. M. Wieland, *Phys. Rev. Lett.* **50**, 503 (1983).
- ⁷ R. D. Sydora, J. N. Leboeuf, Z. G. An, P. H. Diamond, G. S. Lee, and T. S. Hahm, *Phys. Fluids* (in press).
- ⁸ L. Garcia, P. H. Diamond, B. A. Carreras, and J. D. Callen, *Phys. Fluids* **28**, 2147 (1985).
- ⁹ G. S. Lee and P. H. Diamond, *Phys. Fluids* (in press).
- ¹⁰ H. R. Strauss, *Phys. Fluids* **20**, 1354 (1977).
- ¹¹ J. M. Greene and J. L. Johnson, *Phys. Fluids* **4**, 875 (1961).
- ¹² L. Garcia, H. R. Hicks, B. A. Carreras, L. A. Charlton, and J. A. Holmes, *J. Comput. Phys.* **65**, 253 (1986).

INTERNAL DISTRIBUTION

- | | | | |
|------|-------------------|--------|---|
| 1. | L. A. Berry | 19. | J. F. Lyon |
| 2. | D. G. Cacuci | 20. | Y-K. M. Peng |
| 3-7. | B. A. Carreras | 21. | K. C. Shaing |
| 8. | L. A. Charlton | 22. | D. A. Spong |
| 9. | N. Dominguez | 23. | J. Sheffield |
| 10. | R. A. Dory | 24-25. | Laboratory Records Department |
| 11. | J. L. Dunlap | 26. | Laboratory Records, ORNL-RC |
| 12. | H. H. Haselton | 27. | Document Reference Section |
| 13. | P. N. Haubenreich | 28. | Central Research Library |
| 14. | C. L. Hedrick | 29. | Fusion Energy Division Library |
| 15. | J. T. Hogan | 30-31. | Fusion Energy Division Publications
Office |
| 16. | J. A. Holmes | 32. | ORNL Patent Office |
| 17. | G. S. Lee | | |
| 18. | M. S. Lubell | | |

EXTERNAL DISTRIBUTION

33. L. Garcia Gonzalo, Dpto. Fisica Teorica, Facultad Ciencias Fisica, Universidad Complutense, E-28040 Madrid, Spain
34. P. H. Diamond, Institute for Fusion Studies, University of Texas, Austin, TX 78712
35. Office of the Assistant Manager for Energy Research and Development, U.S. Department of Energy, Oak Ridge Operations Office, P.O. Box E, Oak Ridge, TN 37831
36. J. D. Callen, Department of Nuclear Engineering, University of Wisconsin, Madison, WI 53706-1687
37. J. F. Clarke, Director, Office of Fusion Energy, Office of Energy Research, ER-50 Germantown, U.S. Department of Energy, Washington, DC 20545
38. R. W. Conn, Department of Chemical, Nuclear, and Thermal Engineering, University of California, Los Angeles, CA 90024
39. S. O. Dean, Fusion Power Associates, 2 Professional Drive, Suite 248, Gaithersburg, MD 20879
40. H. K. Forsen, Bechtel Group, Inc., Research Engineering, P.O. Box 3965, San Francisco, CA 94105
41. J. R. Gilleland, GA Technologies, Inc., Fusion and Advanced Technology, P.O. Box 81608, San Diego, CA 92138

42. R. W. Gould, Department of Applied Physics, California Institute of Technology, Pasadena, CA 91125
43. R. A. Gross, Plasma Research Laboratory, Columbia University, New York, NY 10027
44. D. M. Meade, Princeton Plasma Physics Laboratory, P.O. Box 451, Princeton, NJ 08544
45. M. Roberts, International Programs, Office of Fusion Energy, Office of Energy Research, ER-52 Germantown, U.S. Department of Energy, Washington, DC 20545
46. W. M. Stacey, School of Nuclear Engineering and Health Physics, Georgia Institute of Technology, Atlanta, GA 30332
47. D. Steiner, Nuclear Engineering Department, NES Building, Tibbetts Avenue, Rensselaer Polytechnic Institute, Troy, NY 12181
48. R. Varma, Physical Research Laboratory, Navrangpura, Ahmedabad 380009, India
49. Bibliothek, Max-Planck Institut fur Plasmaphysik, D-8046 Garching, Federal Republic of Germany
50. Bibliothek, Institut fur Plasmaphysik, KFA, Postfach 1913, D-5170 Julich, Federal Republic of Germany
51. Bibliotheque, Centre des Recherches en Physique des Plasmas, 21 Avenue des Bains, 1007 Lausanne, Switzerland
52. F. Prevot, CEN/Cadarache, Departement de Recherches sur la Fusion Controlee, 13108 Saint-Paul-lez-Durance Cedex, France
53. Documentation S.I.G.N., Departement de la Physique du Plasma et de la Fusion Controlee, Centre d'Etudes Nucleaires, B.P. 85, Centre du Tri, 38041 Grenoble Cedex, France
54. Library, Culham Laboratory, UKAEA, Abingdon, Oxfordshire, OX14 3DB, England
55. Library, FOM-Instituut voor Plasma-Fysica, Rijnhuizen, Edisonbaan 14, 3439 MN Nieuwegein, The Netherlands
56. Library, Institute of Plasma Physics, Nagoya University, Nagoya 464, Japan
57. Library, International Centre for Theoretical Physics, P.O. Box 586, I-34100 Trieste, Italy
58. Library, Laboratorio Gas Ionizzati, CP 56, I-00044 Frascati, Rome, Italy
59. Library, Plasma Physics Laboratory, Kyoto University, Gokasho, Uji, Kyoto, Japan
60. Plasma Research Laboratory, Australian National University, P.O. Box 4, Canberra, A.C.T. 2000, Australia
61. Thermonuclear Library, Japan Atomic Energy Research Institute, Tokai Establishment, Tokai-mura, Naka-gun, Ibaraki-ken, Japan
62. G. A. Eliseev, I. V. Kurchatov Institute of Atomic Energy, P.O. Box 3402, 123182 Moscow, U.S.S.R.

63. V. A. Glukhikh, Scientific-Research Institute of Electro-Physical Apparatus, 188631 Leningrad, U.S.S.R.
64. I. Shpigel, Institute of General Physics, U.S.S.R. Academy of Sciences, Ulitsa Vavilova 38, Moscow, U.S.S.R.
65. D. D. Ryutov, Institute of Nuclear Physics, Siberian Branch of the Academy of Sciences of the U.S.S.R., Sovetskaya St. 5, 630090 Novosibirsk, U.S.S.R.
66. V. T. Tolok, Kharkov Physical-Technical Institute, Academical St. 1, 310108 Kharkov, U.S.S.R.
67. Library, Academia Sinica, P.O. Box 3908, Beijing, China (PRC)
68. D. H. Crandall, Experimental Plasma Research Branch, Division of Development and Technology, Office of Fusion Energy, Office of Energy Research, ER-542 Germantown, U.S. Department of Energy, Washington, DC 20545
69. N. A. Davies, Office of the Associate Director, Office of Fusion Energy, Office of Energy Research, ER-51 Germantown, U.S. Department of Energy, Washington, DC 20545
70. D. B. Nelson, Director, Division of Applied Plasma Physics, Office of Fusion Energy, Office of Energy Research, ER-54 Germantown, U.S. Department of Energy, Washington, DC 20545
71. E. Oktay, Division of Confinement Systems, Office of Fusion Energy, Office of Energy Research, ER-55 Germantown, U.S. Department of Energy, Washington, DC 20545
71. W. Sadowski, Fusion Theory and Computer Services Branch, Division of Applied Plasma Physics, Office of Fusion Energy, Office of Energy Research, ER-541 Germantown, U.S. Department of Energy, Washington, DC 20545
73. P. M. Stone, Fusion Systems Design Branch, Division of Development and Technology, Office of Fusion Energy, Office of Energy Research, ER-532 Germantown, U.S. Department of Energy, Washington, DC 20545
74. J. M. Turner, International Programs, Office of Fusion Energy, Office of Energy Research, ER-522 Germantown, U.S. Department of Energy, Washington, DC 20545
75. R. E. Mickens, Atlanta University, Department of Physics, Atlanta, GA 30314
76. M. N. Rosenbluth, RLM 11.218, Institute for Fusion Studies, University of Texas, Austin, TX 78712
77. Duk-In Choi, Department of Physics, Korea Advanced Institute of Science and Technology, P.O. Box 150, Chong Ryang-Ri, Seoul, Korea
78. D. G. Swanson, Auburn University, Auburn, AL 36849
79. Theory Department Read File, c/o D. W. Ross, University of Texas, Institute for Fusion Studies, Austin, TX 78712

80. Theory Department Read File, c/o R. C. Davidson, Director, Plasma Fusion Center, NW 16-202, Massachusetts Institute of Technology, Cambridge, MA 02139
81. Theory Department Read File, c/o R. White, Princeton Plasma Physics Laboratory, P.O. Box 451, Princeton, NJ 08544
82. Theory Department Read File, c/o L. Kovrizhnykh, Lebedev Institute of Physics, Academy of Sciences, 53 Leninsky Prospect, 117924 Moscow, U.S.S.R.
83. Theory Department Read File, c/o B. B. Kadomtsev, I. V. Kurchatov Institute of Atomic Energy, P.O. Box 3402, 123182 Moscow, U.S.S.R.
84. Theory Department Read File, c/o T. Kamimura, Institute of Plasma Physics, Nagoya University, Nagoya 464, Japan
85. Theory Department Read File, c/o C. Mercier, Departement de Recherches sur la Fusion Controlee, B.P. No. 6, F-92260 Fontenay-aux-Roses (Seine), France
86. Theory Department Read File, c/o T. E. Stringer, JET Joint Undertaking, Culham Laboratory, Abingdon, Oxfordshire OX14 3DB, England
87. Theory Department Read File, c/o R. Briscoe, Culham Laboratory, Abingdon, Oxfordshire OX14 3DB, England
88. Theory Department Read File, c/o D. Biskamp, Max-Planck-Institut fur Plasmaphysik, D-8046 Garching, Federal Republic of Germany
89. Theory Department Read File, c/o T. Takeda, Japan Atomic Energy Research Institute, Tokai Establishment, Tokai-mura, Naka-gun, Ibaraki-ken, Japan
90. Theory Department Read File, c/o J. Greene, GA Technologies, Inc., P.O. Box 81608, San Diego, CA 92138
91. Theory Department Read File, c/o L. D. Pearlstein, L-630, Lawrence Livermore National Laboratory, P.O. Box 5511, Livermore, CA 94550
92. Theory Department Read File, c/o R. Gerwin, CTR Division, Los Alamos National Laboratory, P.O. Box 1663, Los Alamos, NM 87545
- 93-243. Given distribution according to TID-4500, Magnetic Fusion Energy (Category Distribution UC-20 g, Theoretical Plasma Physics)